von Karman Institute for Fluid Dynamics
Chaussée de Waterloo, 72
B - 1640 Rhode Saint Genèse - Belgium

Stagiaire report September 1999

TIME ACCURATE SOLUTION OF HYPERBOLIC PARTIAL DIFFERENTIAL EQUATIONS USING FCT AND RESIDUAL DISTRIBUTION

Mario Ricchiuto

Supervisor:H. Deconinck

Table of Contents

Abstract

A second order Lax Wendroff timestepping approach has been implemented in the in-house 2-D solver "IcARus". It has been tested on several scalar 1-D and 2-D problems and on two Euler testcases. Comparisons have been carried out with an earlier implicit approach using a consistent mass matrix formulation. Fair agreement between the explicit and implicit results was found, although the latter were always better.For the scalar testcases, monotonic results are obtained by a blending of the second order scheme with a monotone first order scheme based on the Flux Corrected Transport (FCT) approach.For the Euler both methods still suffer from a lack of monotonicity, and suggestions are made to improve it.

Acknowledgements

First of all i would like to thank all the stagiaires for making this summer so great:

-Thank you Pietro and Tiziano for working until late in the computer center like me (but probably you worked more than me),Andrea for being so shy,Carlos for teaching me that life must be enjoyed, Joe for the long talks about everything, Gazi for being so good and kind, Todd for correcting my report, Timo for being such a good beer-mate (and of course for your car), Laura for being so nice, Ioanna for being so fascinating, Ozhan for teaching us the turkish swear-words, Miguel for trusting in my advises, Leonardo for being so funny, Claudio for not getting drunk in the canteen, Ewin for his advises on religion and A.J, Carstsen, Enrique, Carla, Jose', Ricardo, Magnus, Egemin for the good time we had together.

Thank you also to Kurt for being so patient everytime i was asking if i had to leave the door open, closed or half open, for all the help he gave me, and for the long talks about CFD.

Thank you David (now i really want to know something more about plasma flows), Patrick, Murat, Michail and Michalis for being so kind and helping me sometimes. Thank you also to Telis who will pick me up at the airport next year.

A really big thank you to professor Deconinck for helping me to learn so much thing in only two months and for trusting in my work, i hope we'll work together again really soon.

Thank you Riccardo and good luck for your D.C., we'll meet soon in Napoli or Potenza.

Thank you to my italian friends for keeping in touch: -Thank you Ciccio, Annarita, Robby, Carmen, Gabry, Serena and Nadia.

A really big, big kiss to Flaviana.

Then i would like to thank my italian professors Nino and Bonfiglioli who gave me the possibility of having such a good experience and thank you to professor Magi for keeping in touch.

Of course i want to thank mamma, papa', Ornella and nonna for loving me so much (I missed you!!).

Again thank you to Aldo Bonfiglioli for teaching me so many things about fluctuation splitting schemes before i came here, without him probably only five pages of this report would exist.

Ciao Nonno !!

List of Symbols

Superscripts

h	: high order
inc	: inconsistent
L	: lumped
l	: low order
lim	: limited
T	: triangular element

Subscripts

H, L	: high order, low order
i, j, l	: indices
R, L	: right, left

Greek symbols

Ω	: domain
β_i	: distribution coefficients
ω	: weighting function
ϕ	: residual
ψ	: limiter
$\vec{\lambda}$	: velocity vector
φ	: limiter function
$\mathbf{\Phi}$	: system residual

Alphanumeric Symbols

$\mathbf{B}$	: distribution matrix
$\mathbf{J}$	: Jacobian of the residual
$\mathbf{M}, m_{ij}$	: mass matrix
R	: Residual vector
$\vec{n}_i$	: edge normal vectors
$\mathbf{A}, \mathbf{B}$	: Jacobians
$\mathbf{F}, \mathbf{G}$	: inviscid fluxes

$\mathbf{I}$	: identical matrix
$\mathbf{Q}$	: symmetrizing variables
$\mathbf{U}$	: conservative variables
c	: speed of sound
k	: inflow parameter
S	: element area
t	: time
u	: solution variable
x, y	: space coordinates

1. INTRODUCTION

Over the last years, a class of multidimensional upwind schemes also known as residual distribution or fluctuation splitting schemes, have been developed at VKI and at the University of Michigan.

Although second order accurate at steady state for homogeneous problems, $\mathcal{LP}$ schemes become only first-order accurate in space for unsteady computations.

To overcome this problem a finite element interpretation with consistent mass matrix was introduced in [1], and the method was shown to be third order accurate in 1-D via a modified equation analysis. In the same work several schemes were tested in their consistent formulation on a scalar 2-D problem. Second order of accuracy was demonstrated using a grid convergence study.

Once a high order of accuracy was recovered, a new problem had to be solved: since the consistent mass matrix is not positive definite, all the consistent schemes showed an oscillating behavior also in the computation of continuous solutions, so the positivity was to be recovered.

The FCT procedure In [3] a way to improve the stability of time accurate methods, the Flux Corrected Transport algorithm (FCT), was introduced for scalar advection equations, and in [4] this technique was generalized to multidimensional problems. The FCT technique is based on the idea of combining the monotonicity of a low order scheme, to prevent spurious oscillations especially near shocks, and the accuracy of a high order scheme, to prevent the smearing of discontinuous solutions typical of first order schemes.

These concepts have been reintroduced by Ferrante in [2] to cure the non monotonicity of the consistent schemes and at the same time a cell based limiting procedure was developed in order to implement the FCT in a residual distribution environment.

Let U be the vector of unknowns and define the time increment of U as

$$\Delta U = U^{n+1} - U^n \tag{1.1}$$

where U^{n+1} and U^n are the values of the variable at time levels n and n+1. In order to have a solution as high order as possible while retaining a monotone behavior, the FCT procedure acts as follows

$$\Delta U = \Delta U^l + (\Delta U^h - \Delta U^l)^{lim} \tag{1.2}$$

where ΔU^l and ΔU^h are the time increments computed respectively with a low order monotone scheme and with a high order scheme; the superscript lim indicates that the difference between the two increments is limited in such a way that no undesired overshoots or undershoots are produced in the solution at the new time level. The preceding equation can be

rewritten as

$$U^{n+1} = U^l + (\Delta U^h - \Delta U^l)^{lim} \tag{1.3}$$

where U^l is the new updated solution obtained using only the low order scheme. To implement this procedure in a cell-vertex residual distribution approach, a slightly different definition of the procedure has to be given, i.e.

$$U_i^{n+1} = U_i^l + \sum_T (\Delta U_i^{h,T} - \Delta U_i^{l,T})^{lim} \tag{1.4}$$

where the subscript i indicates that the value at node i of the variables is considered, while the summation extends over all the triangles meeting at node i.

An algorithm for the implementation of FCT on a solver is given by the following steps:

1. Compute $\Delta U_i^{l,T}$: the "Low order Element Contribution from triangle T to node i", from some low order scheme that guarantees monotonic results.
2. Compute $\Delta U_i^{h,T}$: the "High order Element Contribution from triangle T to node i", from a high order scheme.
3. Define AEC_i^T: the "Antidiffusive Element Contribution from triangle T to node i":

$$AEC_i^T = \Delta U_i^{h,T} - \Delta U_i^{l,T} \tag{1.5}$$

4. Compute the update for the low order solution for node i:

$$U_i^l = U_i^n + \sum_T \Delta U_i^{l,T} = U_i^n + \Delta U_i^l \tag{1.6}$$

5. Limit or "correct" the AEC_i^T so that U^{n+1} computed in the next step is free of extrema not also found in U^l or U^n:

$$AEC_i^{T,lim} = \psi^T * AEC_i^T, \qquad 0 \leq \psi^T \leq 1 \tag{1.7}$$

6. Apply the limited $AEC_i^{T,lim}$ for the update:

$$U_i^{n+1} = U_i^l + \sum_T AEC_i^{T,lim} \tag{1.8}$$

The FCT procedure was included in the 2-D solver IcARus by Ferrante only for implicit computations with the following steps:

1. Compute ΔU^h, the global high order increment, using Crank-Nicolson time integration and the consistent mass matrix (see sect. 2.1) assembled from the local element contributions:
$$(\frac{M}{\Delta t} + \frac{J}{2})\Delta U^h = -R^h \tag{1.9}$$
$$M_H \Delta U^h = -R^h \tag{1.10}$$
ΔU^h is stored.

2. Compute ΔU^l, the global low ($1st$) order increment, that guarantees monotonic results, using the inconsistent mass matrix formulation (see sect. 2.1) and Explicit Euler time integration:
$$S_i \frac{\Delta U_i^l}{\Delta t} = -R_i^l \tag{1.11}$$
or in global notation:
$$M_L \Delta U^l = -R^l \tag{1.12}$$
where M_L is the diagonal lumped mass matrix (see sect. 2.1).

3. Compute the low order update and store it:
$$U^l = U^n + \Delta U^l \tag{1.13}$$

4. Split AEC, the nodal antidiffusive correction:
$$AEC = \Delta U^h - \Delta U^l \tag{1.14}$$
in element contributions. From (1.10) and (1.12) one has:
$$M_L(\Delta U^h - \Delta U^l) = R^l - R^h + (M_L - M_H)\Delta U^h, \tag{1.15}$$
and splitting in element contributions gives:
$$M_L \sum_T (AEC_i^T) = \sum_T (R^{l,T} - R^{h,T}) + \sum_T (M_L^T - M_H^T)\Delta U^h. \tag{1.16}$$
So, locally to the triangle T:
$$AEC^T = M_L^{-1}\left(R^{l,T} - R^{h,T} + \left(M_L^T - M_H^T\right)\Delta U^h\right) \tag{1.17}$$
and it is easy to verify that
$$\sum_T AEC^T = AEC \tag{1.18}$$
is satisfied. So, for each node i of the triangle T:
$$AEC_i^T = \frac{\Delta t}{S_i}\left\{R_i^{l,T} - R_i^{h,T} + \left[\left(M_L^T - M_H^T\right)\Delta U^h\right]_i\right\} \tag{1.19}$$

5. Limit or "correct" the AEC_i^T such that U^{n+1}, computed in the next step, is free of extrema not also found in U^l or U^n:

$$AEC_i^{T,lim} = \psi^T * AEC_i^T, \quad 0 \leq \psi^T \leq 1 \tag{1.20}$$

6. Apply the limited $AEC_i^{T,lim}$ for the update:

$$U_i^{n+1} = U_i^l + \sum_T AEC_i^{T,lim} \tag{1.21}$$

It is clear that the critical point is the limiting step, in [2] the following procedure was used and, at least for scalar problems, fully monotone results were obtained:

1. Compute the maximum (minimum) nodal value U between U^n and U^l:

$$U_i^* = \begin{cases} \max \\ \min \end{cases} (U_i^l, U_i^n) \tag{1.22}$$

2. Compute the maximum (minimum) nodal value of elements T:

$$U_T^* = \begin{cases} \max \\ \min \end{cases} (U_A^*, U_B^*, U_C^*) \tag{1.23}$$

   where A, B, C represents the nodes of element T

3. Compute the maximum (minimum) U of all elements surrounding node i, node i included:

$$U_i^{\begin{smallmatrix}\max\\ \min\end{smallmatrix}} = \begin{cases} \max \\ \min \end{cases} (U_1^*, U_2^*, ..., U_m^*) \tag{1.24}$$

   where $1, 2, ..., m$ represent the elements surrounding node i;

4. Compute the node-cell limiter:

$$\psi_p^T = \frac{U_p^{max} - U_p^l}{\sum_{T \in \mathcal{D}(p)} max(0, (U_p^h - U_p^l)^T)} \tag{1.25}$$

   $p = i, j, k$ represents the nodes of the cell T

5. Compute the cell limiter as the minimum on the nodes:

$$\psi^T = \min_{p=i,j,k} (\psi_p^T) \tag{1.26}$$

More recently in [5] an alternative way was suggested to improve the accuracy in the computation of the solution of time dependent advection problems. The use of a second order time accurate scheme based on a time Lax Wendroff time-stepping is proposed, and monotonicity is ensured by the use of an FCT procedure. Goal of the present work is to further investigate this approach, to implement the time accurate Lax Wendroff scheme in the IcARus solver and to compare the results with the implicit consistent formulation used in [2].

Part I

The 1-D and 2-D convection equation

2. FLUCTUATION SPLITTING SCHEMES ON TRIANGULAR MESHES

In the first part of this work, the homogeneous advection equation in 1-D and 2D,

$$\frac{\partial u}{\partial t} + \vec{\lambda} \cdot \vec{\nabla} u = 0, \tag{2.1}$$

is solved by residual distribution methods. The solution is approximated continuously over the elements by piecewise linear (P1) shape functions.

The cell "fluctuation" ϕ^T is defined as

$$\phi^T = -\int_{\Omega_T} \frac{\partial u}{\partial t}\, d\Omega = \int_{\Omega_e} \vec{\lambda} \cdot \vec{\nabla} u \; d\Omega \tag{2.2}$$

The nodal residual is then computed by re-distributing (splitting) the fluctuation to the vertices of the cell by distribution coefficients β_i:

$$R_i = \sum_T \beta_i^T \phi^T = \sum_T \phi_i^T. \tag{2.3}$$

For consistency, the β_i^T must sum up to one within an element.

The general semi-discretization of equation (2.1) is then:

$$\sum_T \sum_j m_{ij}^T \frac{du_j}{dt} + \sum_T \beta_i^T \phi^T = 0 \tag{2.4}$$

where in the first term on the left hand side a generic mass matrix appears (see sect. 2.1).

For the actual distribution, an inflow parameter $k_l = \frac{1}{2}\, \vec{\lambda} \cdot \vec{n_l}$ is defined (fig. 2.1), where $\vec{n_l}$ is the scaled inward normal on the corresponding side.

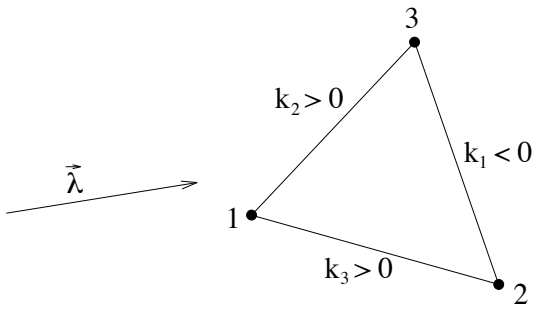

Fig. 2.1 – Definition of inflow parameters

Using these concepts we can design schemes such that they satisfy certain desirable properties:

- Upwinding ($\mathcal{U}$): A scheme is said to be upwind when contributions are only distributed to nodes opposite an inflow edge, i.e. to downstream nodes:

$$k_l \leq 0 \Leftrightarrow \beta_l = 0 \tag{2.5}$$

- Positivity ($\mathcal{P}$): Writing the nodal residual contribution as

$$\phi_i^T = \beta_i^T \phi^T = \sum_j C_{ij}^T u_j, \tag{2.6}$$

  a scheme is locally positive when $C_{ij} \leq 0 \; \forall j \neq i$ and $C_{ii} \geq 0$. The positivity property guarantees that no new local extrema are formed in the solution and therefore precludes spurious oscillations.

- Linearity Preservation ($\mathcal{LP}$): A scheme is said to possess the $\mathcal{LP}$ property if the distribution coefficients β_i^T remain bounded for $\phi^T \to 0$.

Godunov's theorem states that linear schemes (i.e. schemes for which the distribution does not depend on the solution itself) cannot be $\mathcal{LP}$ and $\mathcal{P}$ at the same time.

2.1 Mass matrix formulations

For the mass matrix in equation 2.4 two different formulations have been used in this work: consistent and inconsistent. The latter is the one mostly used for steady state computations, even when implicit time integration is used.

The consistent mass matrix has been derived in [1] based on a finite element interpretation of the residual distribution schemes.It is defined by the following integral:

$$m_{ij}^T = \int \int_{S_T} \omega_i N_j d\Omega \tag{2.7}$$

where N_j is the linear shape function used to approximate the solution and the test function ω_i is defined as follows:

$$\omega_i = N_i + \beta_i^T - \frac{1}{3}. \tag{2.8}$$

Integration of the right hand side of equation 2.7 leads to the consistent mass matrix:

$$m_{ij}^T = \frac{S_T}{3} \cdot \begin{bmatrix} \frac{1}{2} + \beta_1^T - \frac{1}{3} & \frac{1}{4} + \beta_1^T - \frac{1}{3} & \frac{1}{4} + \beta_1^T - \frac{1}{3} \\ \frac{1}{4} + \beta_2^T - \frac{1}{3} & \frac{1}{2} + \beta_2^T - \frac{1}{3} & \frac{1}{4} + \beta_2^T - \frac{1}{3} \\ \frac{1}{4} + \beta_3^T - \frac{1}{3} & \frac{1}{4} + \beta_3^T - \frac{1}{3} & \frac{1}{2} + \beta_3^T - \frac{1}{3} \end{bmatrix}. \tag{2.9}$$

The inconsistent mass matrix is obtained by lumping to the diagonal all the elements on a given column:

$$m_{ij}^{L,inc,T} = S_T \cdot \begin{bmatrix} \frac{1}{3} & 0 & 0 \\ 0 & \frac{1}{3} & 0 \\ 0 & 0 & \frac{1}{3} \end{bmatrix} = \frac{S_T}{3}\mathbf{I} \tag{2.10}$$

2.2 Time integration

In the course of this work two time integration strategies will be compared: the implicit Crank-Nicolson time-stepping with consistent mass matrix (equation (2.11)) used by Ferrante in [2] and the explicit Lax Wendroff time-stepping with inconsistent mass matrix proposed in [5] (equation (2.12)):

$$\left[\frac{\mathbf{M}}{\Delta t} + \frac{\mathbf{J}}{2}\right] \Delta U^n = -R^n; \tag{2.11}$$

$$\frac{\mathbf{M}_L}{\Delta t}\Delta U^n = -R^n \tag{2.12}$$

where $\mathbf{J}$ is the jacobian of the residual:

$$[\mathbf{J}]_{ij} = \frac{\partial R_i}{\partial u_j}\Delta u_j. \tag{2.13}$$

2.3 Review of existing space discretization schemes

Here follows a short review of the space discretization schemes previously used and of their properties. In [1] and [2], it was demonstrated that for LP schemes second order of accuracy in time can only be obtained if they are combined with the consistent mass matrix this however makes the schemes implicit in time. A deeper analysis is made on the Lax-Wendroff scheme to show that it could be a possible alternative to the consistent formulation for time accurate computations.

2.3.1 LDA scheme

The "low diffusion A", or LDA scheme is a linear upwind scheme that is linearity preserving and therefore not positive. Its distribution coefficients are:

$$\beta_i^{T,LDA} = \frac{max(0, k_i)}{\sum_j max(0, k_i)} \tag{2.14}$$

Although second order in the steady case this $\mathcal{LP}$ scheme has been shown in [1] to be only first order accurate for time dependent problems if an inconsistent mass matrix is used, so in [2] the consistent formulation was used to build the high order scheme for the FCT procedure.

2.3.2 N scheme

The N (for narrow) scheme is the optimum linear first order positive scheme with respect to minimizing crosswise diffusion. Its fluctuation contributions to the vertices are:

$$\phi_i^{T,N} = -k_i^+ (\sum_j k_j^+)^{-1} \sum_j k_j^- (u_i - u_j), \tag{2.15}$$

where $k_i^+ = max(k_i, 0)$, $k_i^- = min(k_i^-, 0)$.

The N scheme can be proven to be positive [7] and therefore cannot be linearity preserving, so only first order of accuracy can be obtained from it also for steady computations, for this reason it is worthless to try a consistent second order time integration for this scheme, but it can be used as a low order monotone computation in the FCT procedure.

2.3.3 PSI scheme

It can be shown that by applying a limiter function φ, nonlinear monotone $\mathcal{P}$ and $\mathcal{LP}$ schemes can be generated from the underlying linear schemes [7]:

$$\beta_i^T = \varphi \left(\frac{\phi_i^{linear}}{\phi_T} \right) \tag{2.16}$$

Applying the min-mod limiter to the N-scheme defines the PSI (positive streamwise invariant) scheme. Also the PSI scheme shows only first order of accuracy for transient problems when combined with an inconsistent mass matrix, but being positive it can be used as a low order monotone scheme in the FCT procedure. When used in combination with a second order time integration with consistent mass matrix second order of accuracy is obtained but monotonicity is lost due to the non positive definiteness of the inverse mass matrix.

2.4 The time accurate Lax-Wendroff scheme

The fluctuation splitting formulation of the 2-D Lax-Wendroff scheme can be found in [7]; the distribution coefficient for node i is given by:

$$\beta_i^{T,LW} = \frac{1}{3} + \frac{\Delta t}{2S_T} k_i. \tag{2.17}$$

If Δt is a cell based time-step, only first order of accuracy in time is obtained, unless a consistent formulation is used. In the next part of the work this formulation will be called

the local formulation of Lax-Wendroff scheme. The time accurate version of the scheme is produced with the choice $\Delta t_T = \Delta t$, a global time-step deriving from the time discretization.

In one space dimension and on an equally spaced mesh it can be easily proven that this scheme has the following modified equation [8]:

$$u_t + \lambda u_x + \frac{|\lambda|}{6}\Delta x^2 \left(1 - \mathrm{CFL}^2\right) u_{xxx} + ... = 0 \tag{2.18}$$

where $u_t + \lambda u_x = 0$ is the 1-D formulation of equation 2.1 and CFL is the Courant number:

$$\mathrm{CFL} = \frac{\lambda \Delta t}{\Delta x}. \tag{2.19}$$

From the analysis of the modified equation is clear that the scheme is second order in time, but it is important to underline that equation 2.18 can be derived only under the assumption that the time-step present in the Lax-Wendroff dissipation term is equal to the time-step arising from the time discretization. So as previously mentioned this is a necessary condition to have second order of accuracy in time for this scheme.

A similar equation in 2-D can be obtained on a regular mesh like the one in figure 5.6. The configuration considered is depicted in figure 2.2, and $\Delta x = \Delta y = h$ will be assumed .

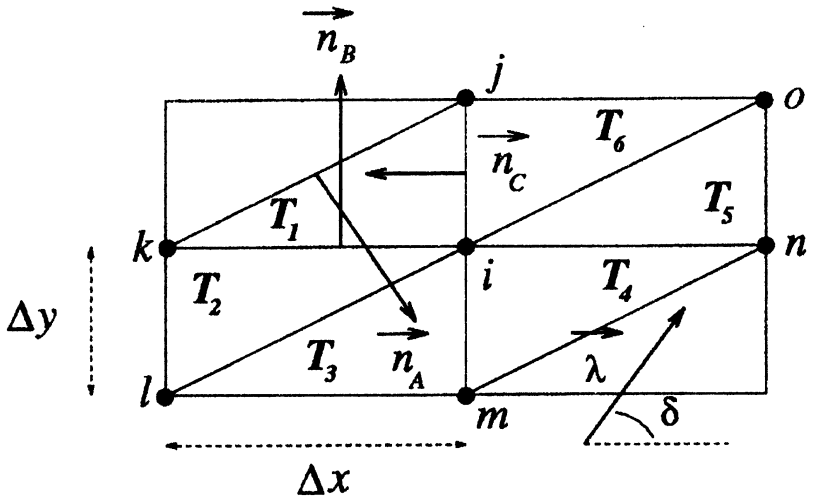

Fig. 2.2 – Regular mesh configuration around node i

For the normals one has:

$$\vec{n}_A = h\,(1\,;\,-1)\,, \quad \vec{n}_B = h\,(0\,;\,1)\,, \quad \vec{n}_C = h\,(-1\,;\,0)\,; \tag{2.20}$$

and for the advection velocity:

$$\vec{\lambda} = \frac{CFL\, h}{\Delta t}\left(\cos\delta\ ;\ \sin\delta\right), \tag{2.21}$$

being Δt the timestep coming from the time discretization and

$$\mathrm{CFL} = \frac{||\vec{\lambda}||\Delta t}{\Delta x}. \tag{2.22}$$

The fluctuations ϕ^{T_i} can be written as:
$\phi^{T_1} = k_A u_i + k_B u_j + k_C u_k$;
$\phi^{T_2} = -k_C u_i - k_A u_k - k_B u_l$;
$\phi^{T_3} = k_B u_i + k_C u_l + k_A u_m$;
$\phi^{T_4} = -k_A u_i - k_B u_m - k_C u_n$;
$\phi^{T_5} = k_C u_i + k_A u_n + k_B u_o$;
$\phi^{T_6} = -k_B u_i - k_C u_o - k_A u_j$;
where
$\mathrm{k}_A = \frac{CFL\, h^2}{2\Delta t}(\cos\delta - \sin\delta)$;
$k_B = \frac{CFL\, h^2}{2\Delta t}\sin\delta$;
$k_C = -\frac{CFL\, h^2}{2\Delta t}\cos\delta$.

Using the notation introduced in the previous lines the Lax Wendroff distribution coefficients can be written as:
$\beta_i^{T_1} = \frac{1}{3} + \frac{CFL\,(\cos\delta - \sin\delta)}{2}$;
$\beta_i^{T_2} = \frac{1}{3} + \frac{CFL\,\cos\delta}{2}$;
$\beta_i^{T_3} = \frac{1}{3} + \frac{CFL\,\sin\delta}{2}$;
$\beta_i^{T_4} = \frac{1}{3} + \frac{CFL\,(-\cos\delta + \sin\delta)}{2}$;
$\beta_i^{T_5} = \frac{1}{3} - \frac{CFL\,\cos\delta}{2}$;
$\beta_i^{T_6} = \frac{1}{3} - \frac{CFL\,\sin\delta}{2}$.
In order to obtain a modified equation the following Taylor expansions around node i are taken, in space:
$\mathrm{u}_l = u_i - hu_x - hu_y + \frac{h^2}{2}u_{xx} + \frac{h^2}{2}u_{yy} + h^2 u_{xy} - \frac{h^3}{6}u_{xxx} - \frac{h^3}{6}u_{yyy} - \frac{h^3}{2}u_{xxy} - \frac{h^3}{2}u_{xyy} + \mathcal{O}(h^4)$;
$u_m = u_i - hu_y + \frac{h^2}{2}u_{yy} - \frac{h^3}{6}u_{yyy} + \mathcal{O}(h^4)$;
$u_n = u_i + hu_x + \frac{h^2}{2}u_{xx} + \frac{h^3}{6}u_{xxx} + \mathcal{O}(h^4)$;
$u_o = u_i + hu_x + hu_y + \frac{h^2}{2}u_{xx} + \frac{h^2}{2}u_{yy} + h^2 u_{xy} + \frac{h^3}{6}u_{xxx} + \frac{h^3}{6}u_{yyy} + \frac{h^3}{2}u_{xxy} + \frac{h^3}{2}u_{xyy} + \mathcal{O}(h^4)$;
$u_j = u_i + hu_y + \frac{h^2}{2}u_{yy} + \frac{h^3}{6}u_{yyy} + \mathcal{O}(h^4)$;
$u_k = u_i - hu_x + \frac{h^2}{2}u_{xx} - \frac{h^3}{6}u_{xxx} + \mathcal{O}(h^4)$;
and in time:
$\mathrm{u}_i^{n+1} = u_i^n + u_t\Delta t + \frac{\Delta t^2}{2}u_{tt} + \frac{\Delta t^3}{6}u_{ttt} + \mathcal{O}(\Delta t^4)$.

The discretized form of equation (2.1) for explicit timestepping with mass lumping is:

$$u_i^{n+1} = u_i^n - \frac{\Delta t}{S_i}\sum_T \beta_i^T \phi^T; \tag{2.23}$$

where the median dual cell area S_i is $S_i = \frac{h^2}{2}$ for the grid chosen.

It is easy to check that the following identities hold:
$\vec{\lambda} \cdot \nabla u = \frac{CFL\, h}{\Delta t} \left(u_x \cos\delta + u_y \sin\delta \right)$;
$\vec{\lambda} \cdot \nabla \left(\vec{\lambda} \cdot \nabla u \right) = \frac{CFL^2\, h^2}{\Delta t^2} \left(u_{xx} \cos^2\delta + u_{yy} \sin^2\delta + 2 u_{xy} \sin\delta \cos\delta \right)$;
$\vec{\lambda} \cdot \nabla \left(u_{xy} + \Delta u \right) = \frac{CFL\, h}{\Delta t} \left(u_{xxx} \cos\delta + u_{xyy} \cos\delta + u_{xxy} \cos\delta + u_{xxy} \sin\delta + u_{xyy} \sin\delta + u_{yyy} \sin\delta \right)$;
where $\Delta(\cdot)$ is the laplacian operator.

Substituting the Taylor expansions in equation (2.23) and using the previous identities, one gets:

$$u_t + \vec{\lambda} \cdot \nabla u = -\frac{\Delta t}{2} u_{tt} + \frac{\Delta t}{2} \vec{\lambda} \cdot \nabla \left(\vec{\lambda} \cdot \nabla u \right) - \frac{\Delta t^2}{6} u_{ttt} - \frac{h^2}{6} \vec{\lambda} \cdot \nabla \left(u_{xy} + \Delta u \right) + \mathcal{O}(\Delta t^3, h^3). \quad (2.24)$$

In order to eliminate the second order time derivative the following procedure can be used:

1. Take the time derivative of equation (2.24) : $(LHS)_t = (RHS)_t \rightarrow$ equation 1;
2. Take the gradient of equation (2.24) : $\nabla (LHS) = \nabla (RHS)$;
3. Multiply by $-\vec{\lambda}$:$-\vec{\lambda} \cdot \nabla (LHS) = -\vec{\lambda} \cdot \nabla (RHS) \rightarrow$ equation 2;
4. Sum equation 1 and equation 2 and solve for u_{tt}.

Following this procedure one obtains:

$$\begin{aligned} -\frac{\Delta t}{2} u_{tt} \;=\; & -\frac{\Delta t}{2} \vec{\lambda} \cdot \nabla \left(\vec{\lambda} \cdot \nabla u \right) + \frac{\Delta t^2}{4} u_{ttt} - \frac{CFL^2\, h^2}{4} \hat{\lambda} \cdot \nabla \left(\hat{\lambda} \cdot \nabla u_t \right) \\ & - \frac{\Delta t\, h\, CFL}{4} \hat{\lambda} \cdot \nabla u_{tt} + \frac{\Delta t\, h^2\, CFL}{4} \hat{\lambda} \cdot \nabla \left[\hat{\lambda} \cdot \nabla \left(\hat{\lambda} \cdot \nabla u \right) \right] \\ & + \mathcal{O}(\Delta t^3, h^3) \end{aligned} \quad (2.25)$$

In the previous equation the CFL number and the unit vector $\hat{\lambda} = \frac{\vec{\lambda}}{||\vec{\lambda}||}$ have been introduced in almost all the terms except the first term on the right hand side to underline the cancellation with the first order term on the right hand side of equation (2.24).

Similarly it can be proven that

$$\begin{aligned} \Delta t^2 u_{ttt} = \quad & CFL^2\, h^2\, \hat{\lambda} \cdot \nabla \left(\hat{\lambda} \cdot \nabla u_t \right) + \mathcal{O}(\Delta t^3, h^3) = \\ & -CFL^2\, h^2\, ||\vec{\lambda}||\, \hat{\lambda} \cdot \nabla \left[\hat{\lambda} \cdot \nabla \left(\hat{\lambda} \cdot \nabla u \right) \right] + \mathcal{O}(\Delta t^3, h^3). \end{aligned} \quad (2.26)$$

Eliminating all the time derivatives and neglecting the higher order terms (i.e. $\mathcal{O}(3)$) the following 2-D modified equation is obtained:

$$u_t + \vec{\lambda} \cdot \nabla u = \frac{||\vec{\lambda}||\, h^2}{6} \left\{ CFL^2\, \hat{\lambda} \cdot \nabla \left[\hat{\lambda} \cdot \nabla \left(\hat{\lambda} \cdot \nabla u \right) \right] - \hat{\lambda} \cdot \nabla \left(u_{xy} + \Delta u \right) \right\} + \mathcal{O}(\Delta t^3, h^3) \quad (2.27)$$

It is easy to verify that in 1-D equation 2.27 reduces to equation 2.18.

So also in 2-D second order of accuracy (at least on the grid considered) should be guaranteed using the Lax Wendroff scheme for discretizing the scalar convection equation.

A 2-D grid convergence study has been made for both a steady and unsteady scalar problem in [6], using the local time-step in the distribution coefficient, while in [5] a similar unsteady testcase has been computed using the time accurate version of the scheme. In both cases explicit time-stepping was used and, although the local formulation gave truly second order of accuracy for the steady computations, only first order for the unsteady case was found, while second order of accuracy was found in [5], confirming the analysis made here.

In the next chapters the use of the time accurate version of the Lax-Wendroff scheme as a possible alternative to the implicit-consistent formulation of $\mathcal{LP}$ schemes for time accurate computations will be tested on several scalar linear and non-linear problems.

3. VALIDATION RESULTS

The 2-D solver IcARus was modified to implement the option for explicit time integration in the unsteady case and the time accurate version of the Lax Wendroff scheme. To check the modifications made, tests were carried out on two scalar testcases and compared with reference [5].

3.1 The rotating cosine hill

The rotating cosine hill is a classical test-case for numerical schemes of the 2D linear unsteady advection equation (2.1). The test consists in the transport in 2D of a "cloud" of cosine shape with a velocity field of constant angular velocity, as shown in figure 3.1. This

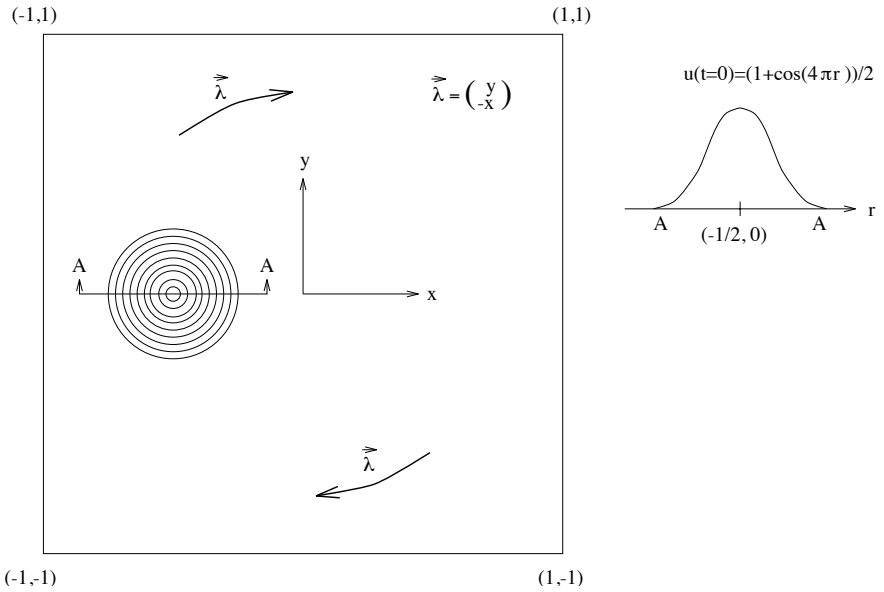

Fig. 3.1 – Rotating cone testcase

testcase was already implemented on IcARus. The only change made was to modify the advection speed to the same form as used in [5]:

$$\vec{\lambda} = [2\pi y, -2\pi x]\,. \tag{3.1}$$

The computation was made on a 64x64 diamond grid (fig. 3.2), fixing the ratio $\frac{\Delta t}{\Delta x} = 0.08$ like in the reference. The results using the Lax Wendroff scheme and explicit time-stepping after one revolution are compared in figures 3.3 and 3.4. Although the height of the hill is well preserved (82% of the initial height) the need of a limiting procedure is clear from figure 3.4 since the solution is not oscillation free.

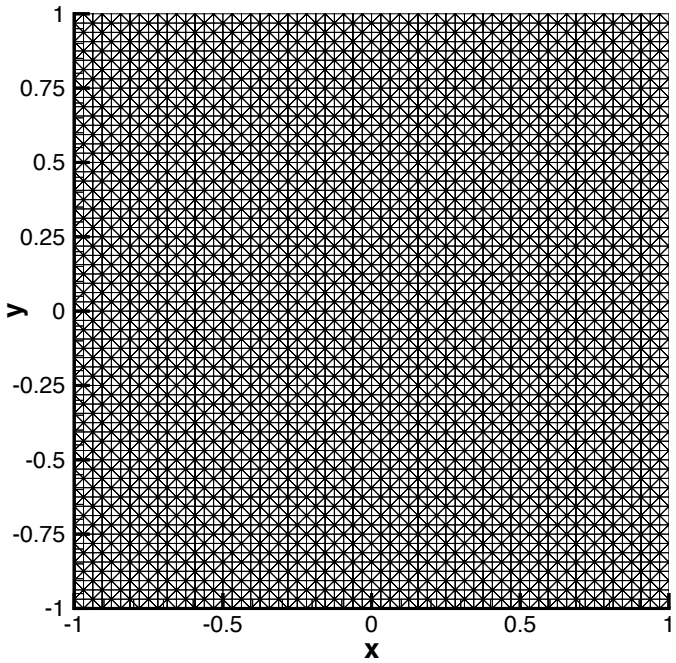

Fig. 3.2 – 64x64 diamond grid

3.2 The rotating cylinder

This testcase differs from the previous only for the initial profile, in fact the initial solution is

$$u_0 = 1 \quad r < 0.25, \tag{3.2}$$

where

$$r = \sqrt{(x + 0.5)^2 + y^2} \tag{3.3}$$

like in the previous testcase. The same advection field of the cosine hill problem is assumed and the computation has been made on the grid of figure 3.2 fixing again the ratio $\frac{\Delta t}{\Delta x} = 0.08$ like in the reference. The results obtained here and in the reference paper are displayed in figure 3.5 and 3.6.

From this testcase it is even more clear than before, that going on with the Lax Wendroff scheme requires a limiting procedure to be implemented: an extension to the explicit inconsistent discretization of the FCT used by Ferrante will be adopted.

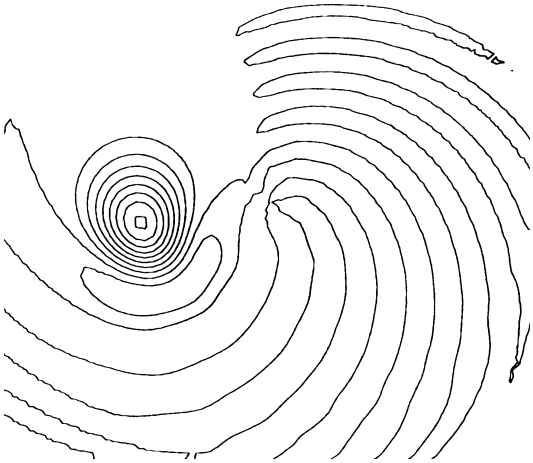

Fig. 3.3 – Cosine hill: solution obtained in reference [5]

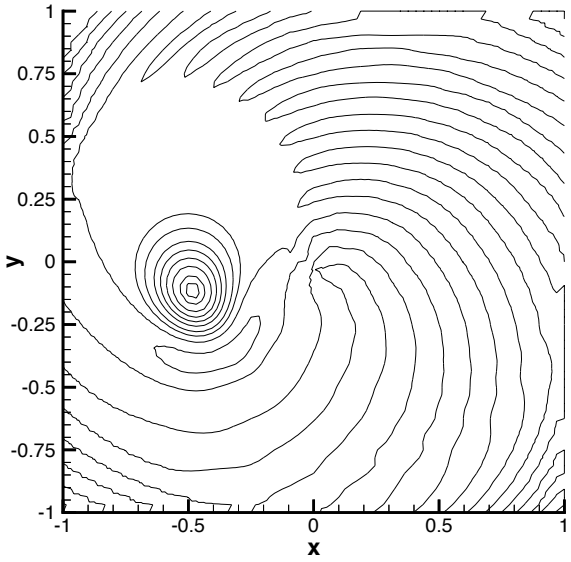

Fig. 3.4 – Cosine hill: solution obtained with IcARus

Fig. 3.5 – Rotating cylinder: solution obtained in reference [5]

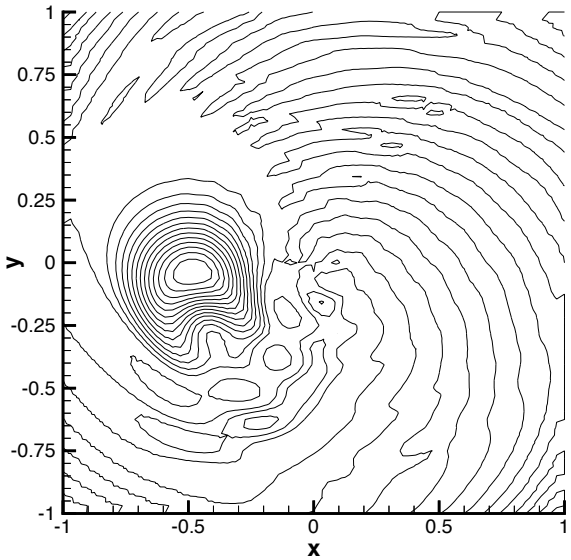

Fig. 3.6 – Rotating cylinder: solution obtained with IcARus

4. FCT PROCEDURE IN THE EXPLICIT INCONSISTENT CASE

To implement the FCT in the explicit inconsistent case the procedure reported in the introduction was slightly modified, but no changes were made to the limiting algorithm. The procedure adopted is the following:

1. Compute ΔU^h and ΔU^l, the global high and low order increment using the explicit lumped formulation:

$$S_i \frac{\Delta U_i^h}{\Delta t} = -R_i^h \tag{4.1}$$

$$S_i \frac{\Delta U_i^l}{\Delta t} = -R_i^l \tag{4.2}$$

or in global notation:

$$M_L \Delta U^h = -R^h \tag{4.3}$$

$$M_L \Delta U^l = -R^l \tag{4.4}$$

ΔU^h and ΔU^l are stored.

2. Compute the low order update and store it:

$$U^l = U^n + \Delta U^l \tag{4.5}$$

3. Split AEC, the nodal antidiffusive correction:

$$AEC = \Delta U^h - \Delta U^l \tag{4.6}$$

in element contributions. From (4.3) and (4.4) it gives:

$$M_L(\Delta U^h - \Delta U^l) = R^l - R^h \tag{4.7}$$

and splitting in element contributions gives:

$$M_L \sum_T (\Delta U^{h,T} - \Delta U^{l,T}) = \sum_T (R^{l,T} - R^{h,T}). \tag{4.8}$$

So for each node i of the triangle T:

$$AEC_i^T = \frac{\Delta t}{S_i} \left\{ R_i^{l,T} - R_i^{h,T} \right\} \tag{4.9}$$

4. Limit or "correct" the AEC_i^T such that U^{n+1}, computed in the next step, is free of extrema not also found in U^l or U^n:

$$AEC_i^{T,lim} = \psi^T * AEC_i^T, \quad 0 \leq \psi^T \leq 1 \tag{4.10}$$

5. Apply the limited $AEC_i^{T,lim}$ for the update:

$$U_i^{n+1} = U_i^l + \sum_T AEC_i^{T,lim} \tag{4.11}$$

It is clear that in the explicit inconsistent case also the FCT procedure is computationally cheaper because no matrix products must be evaluated.

5. RESULTS

As a first test in order to validate the implementation on IcARus of the explicit inconsistent FCT, a comparison is again made with reference [5] where use of the same algorithm is made, but with a slightly less strict limiting algorithm. Then results for several scalar testcases are presented and comparisons are made between the inconsistent formulation using the time accurate Lax Wendroff scheme and the consistent one. The following schemes will be considered:

1. FCT : Lax Wendroff inconsistent as high order and N scheme as low order;
2. FCT : Lax Wendroff inconsistent as high order and PSI scheme as low order;
3. FCT : LDA consistent as high order and N scheme as low order;
4. FCT : LDA consistent as high order and PSI scheme as low order.

The consistent schemes (consistent FCT) will be used in combination with the implicit Crank-Nicholson timestepping, while only explicit timestepping will be adopted for the inconsistent FCT.

5.1 Validation

In figure 5.1, 5.2, 5.3 and 5.4 the results are compared after one revolution for the cosine hill and rotating cylinder testcases, using the grid of figure 3.2. The time accurate version of the Lax Wendroff scheme is used as high order and the PSI scheme as low order method. As noted by the authors of [5] the solutions obtained for the cosine hill with the different limiters are almost indistinguishable, the only difference is in the cone height that is slightly less here (74% instead of 76% of the initial height), but this is natural because of the more strict limiting used. It is interesting to underline that the solution in not only oscillation free, but also the phase lag of the Lax Wendroff scheme is partially corrected in the FCT procedure.

Fig. 5.1 – Cosine hill: solution obtained in reference [5]

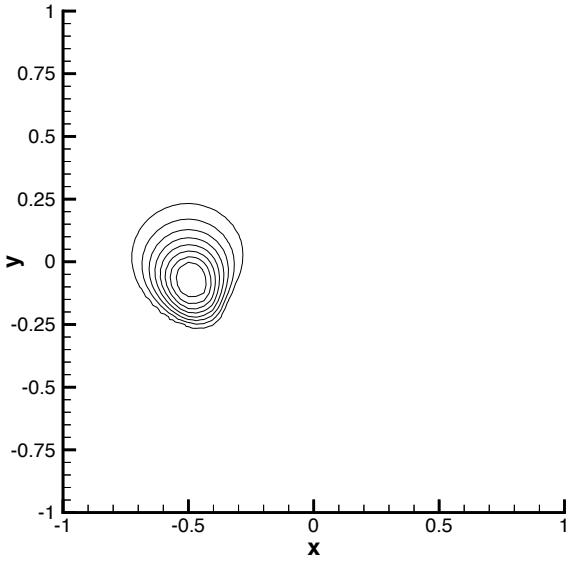

Fig. 5.2 – Cosine hill: solution obtained with IcARus

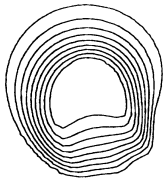

Fig. 5.3 – Rotating cylinder: solution obtained in reference [5]

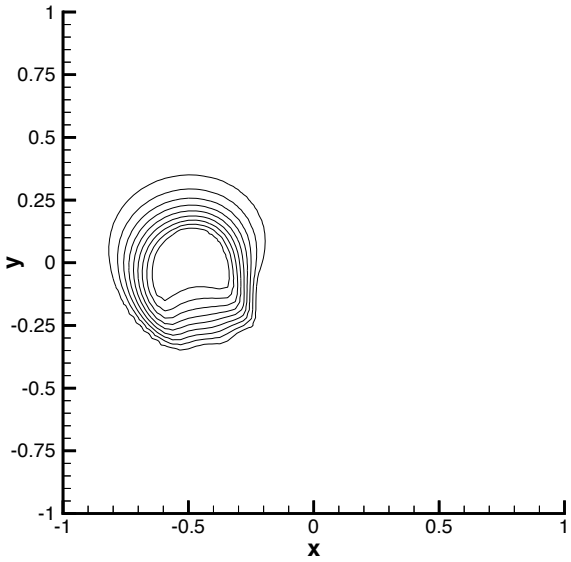

Fig. 5.4 – Rotating cylinder: solution obtained with IcARus

5.2 Rotating cosine hill

As a first step the sensitivity to the mesh topology of the algorithm used was tested running this testcase on three different types of grids:

1. the 80x80 regular grid of figure 5.6;
2. an 80x80 diamond grid;
3. the isotropic grid of figure 5.5 with 80 cells on each boundary.

The results after one revolution are displayed in figures from 5.7 to 5.12. It is clear that the solution obtained is almost the same on these grids, the better result on the isotropic one is mostly due to the fact that although the number of boundary cells is the same of the other grids, the total number of nodes is larger for this one. As expected the use of the PSI as low order scheme gives better results than the use of the N scheme, being the PSI scheme less diffusive.

The results obtained on the 80x80 diamond grid with the consistent implicit formulation are those in figure 5.13 and 5.14. The computations were carried out by fixing the ratio $\frac{\Delta t}{\Delta x} = 0.08$ like in the explicit case. Comparing with figures 5.9 and 5.10 it is evident that the solutions are comparable if the final height of the hill is used to judge their quality. Actually the implicit solutions do not suffer of the phase lag still present in the inconsistent FCT computations, so they are better as can be seen in figures 5.15 and 5.16. Especially the consistent solution obtained using the PSI scheme for the low order computations is a really good one for both the height preserving and global agreement with the exact solution.

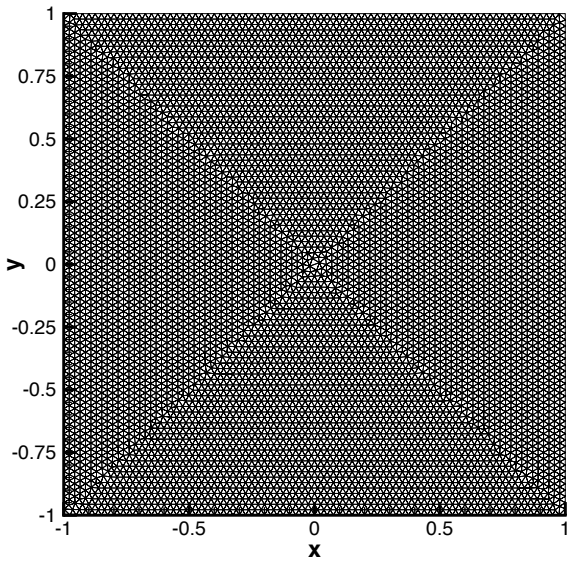

Fig. 5.5 – Isotropic grid

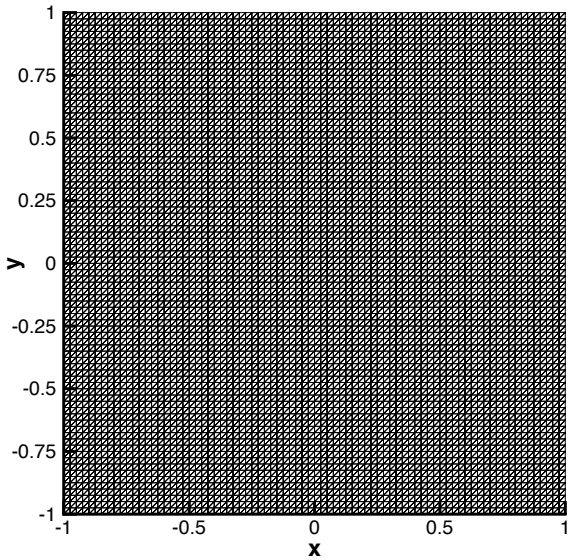

Fig. 5.6 – 80x80 regular grid

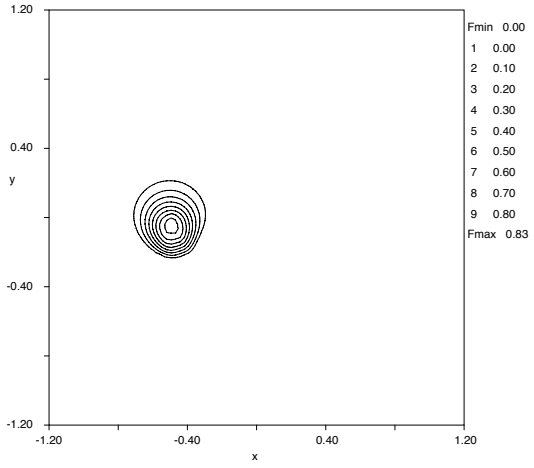

Fig. 5.7 – FCT : L-W inconsistent N inconsistent on the regular grid of fig.5.6

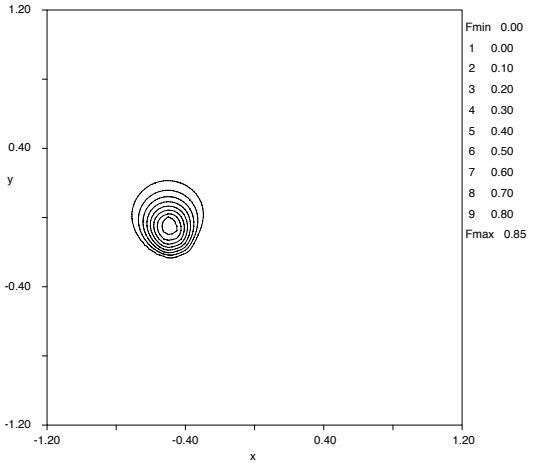

Fig. 5.8 – FCT : L-W inconsistent PSI inconsistent on the regular grid of fig.5.6

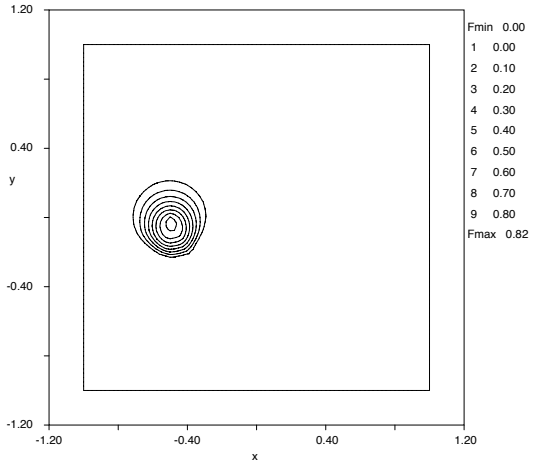

Fig. 5.9 – FCT : L-W inconsistent N inconsistent on the 80x80 diamond grid

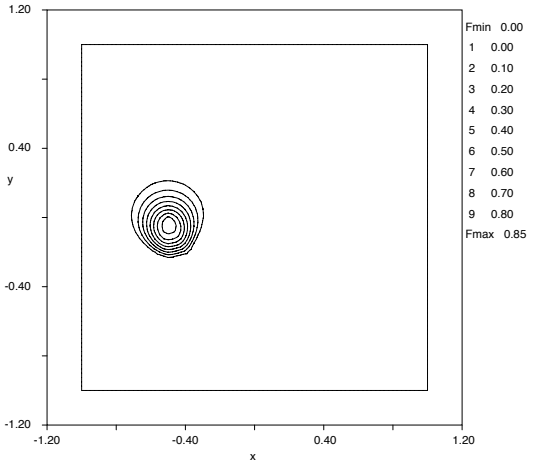

Fig. 5.10 – FCT : L-W inconsistent PSI inconsistent on the 80x80 diamond grid

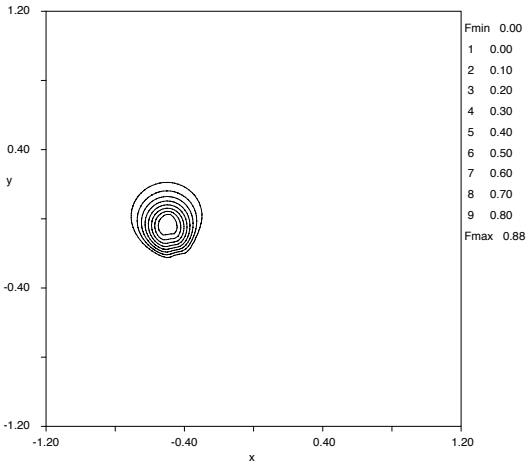

Fig. 5.11 – FCT : L-W inconsistent N inconsistent on the grid of fig.5.5

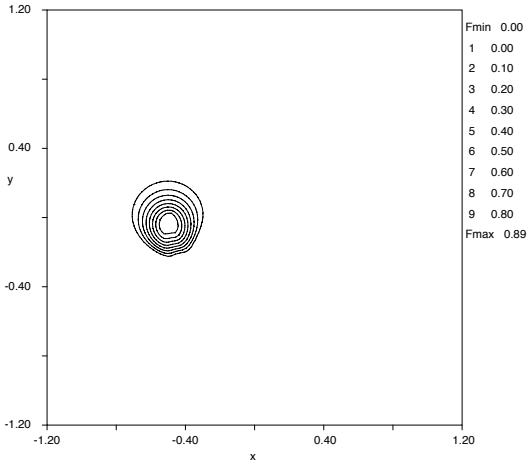

Fig. 5.12 – FCT : L-W inconsistent PSI inconsistent on the grid of fig.5.5

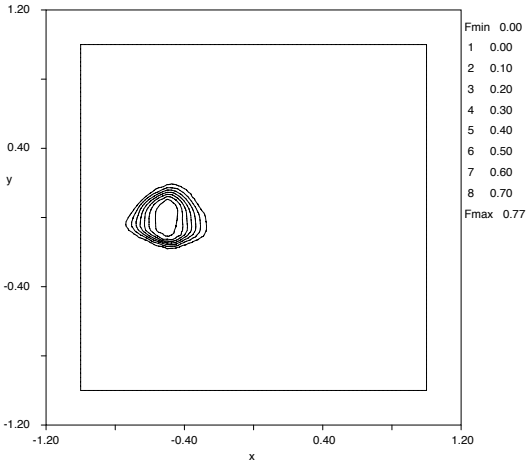

Fig. 5.13 – FCT : LDA consistent and N inconsistent with Crank-Nicolson implicit timestepping

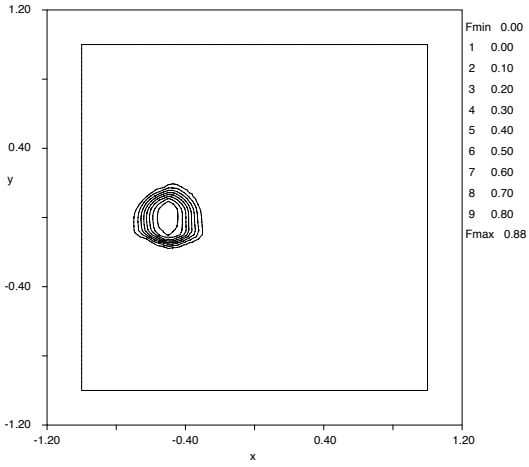

Fig. 5.14 – FCT : LDA consistent and PSI inconsistent with Crank-Nicolson implicit timestepping

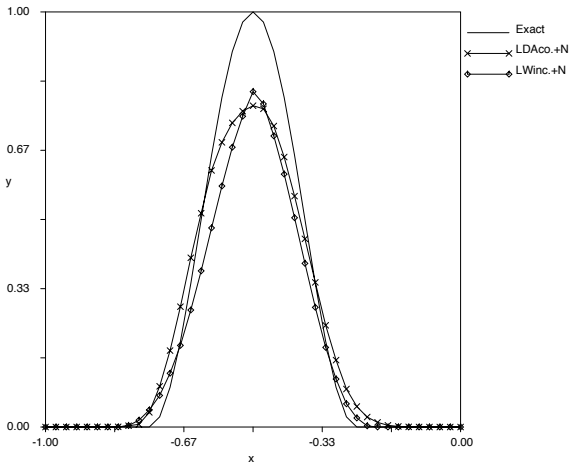

Fig. 5.15 – Sections at $y = 0$ of the solutions obtained using the N scheme as low order scheme

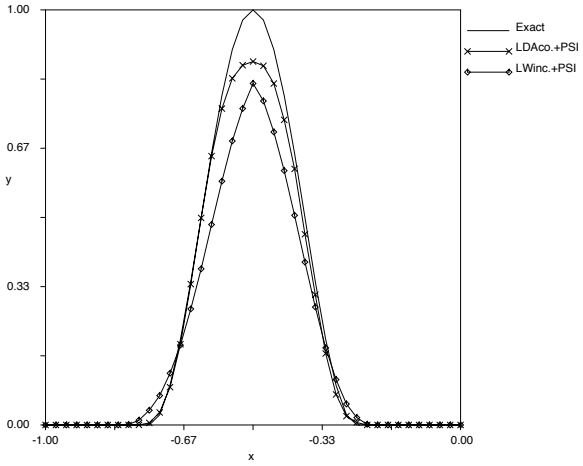

Fig. 5.16 – Sections at $y = 0$ of the solutions obtained using the PSI scheme as low order scheme

5.3 Rotating cylinder

The consistent and inconsistent formulation were compared also on this testcase. The 80x80 diamond grid has been used and the same ratio $\frac{\Delta t}{\Delta x}$ as in the previous case has been fixed. The result after one revolution is displayed in the figures from 5.17 to 5.22. Again the consistent and inconsistent results are close if a section at $y = 0$ is considered, but the former are better because of the complete absence of phase lag like in the rotating cosine hill case. Again the result obtained with consistent formulation and PSI scheme is really good being globally aximmetric. From the results of this testcase it is really evident that a phase lag is still present on the solution obtained using the Lax Wendroff scheme with explicit timestepping and mass lumping. Probably this problem could be cured using a finer grid,but this will make the computation less cheap.

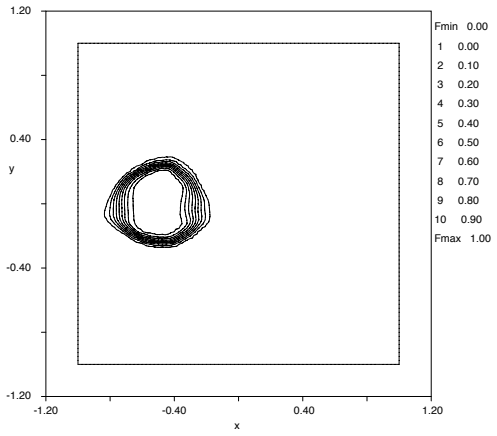

Fig. 5.17 – FCT : LDA consistent and N inconsistent with Crank-Nicolson timestepping

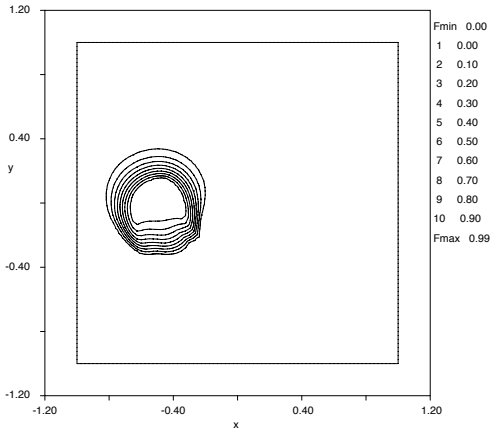

Fig. 5.18 – FCT : L-W inconsistent and N inconsistent

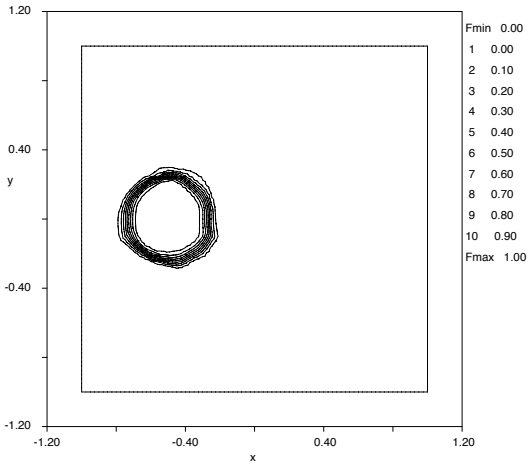

Fig. 5.19 – FCT : LDA consistent and PSI inconsistent with Crank-Nicolson timestepping

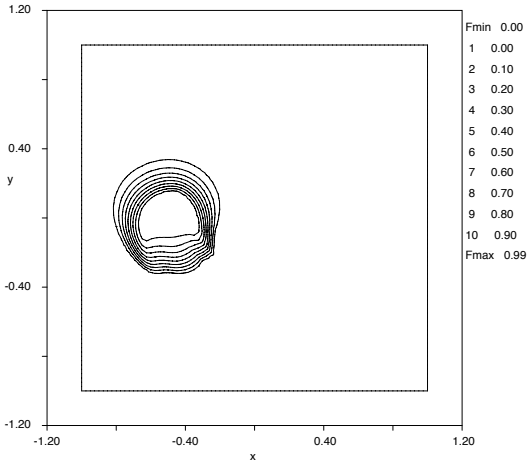

Fig. 5.20 – FCT : L-W inconsistent and PSI inconsistent

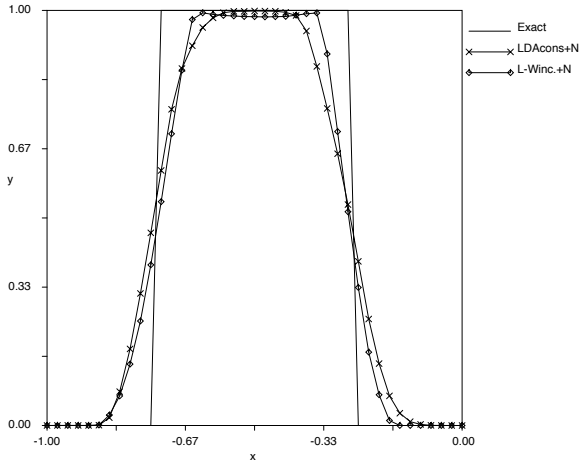

Fig. 5.21 – Sections at $y = 0$ of the solutions obtained using the N scheme as low order scheme

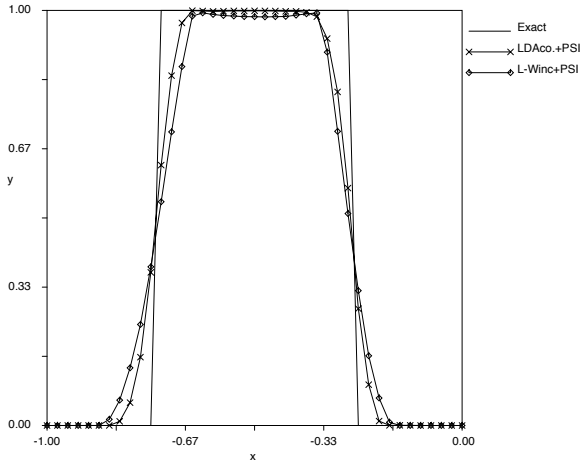

Fig. 5.22 – Sections at $y = 0$ of the solutions obtained using the PSI scheme as low order scheme

5.4 1-D linear step advection

Another typical scalar test-case for numerical schemes is the 1D linear advection of a step function. The equation (2.1) with $\vec{\lambda} = (a, 0)$ gives the 1D linear wave equation:

$$\frac{\partial u}{\partial t} + a\frac{\partial u}{\partial x} = 0 \tag{5.1}$$

where the convection speed a is a constant.

If the following initial solution is given

$$u(x, t = 0) = u_0(x) = f(x) \tag{5.2}$$

the exact solution is

$$u = f(x - at). \tag{5.3}$$

In this section the convection of a discontinuity in the positive x direction is analyzed. The initial condition ($t = 0$) is the following:

$$\begin{cases} u(x,0) = 1 & x < 5 \\ u(x,0) = 0 & x > 5 \end{cases} \tag{5.4}$$

The grid used for this test is a 2D regular triangular mesh with 81x5 points(fig.5.23). The CFL adopted (referred to wave speed $a = 1$) is .95, and the time level at which the solution is shown is 2.95, reached after 25 constant time steps.

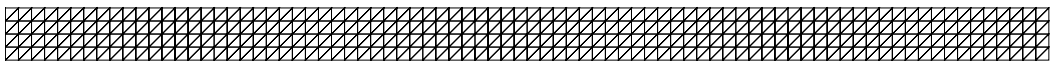

Fig. 5.23 – Grid used for the pseudo 1-D computations

Although the computation was not truly 1-D, all the upwind lumped schemes gave the same solution on this problem (fig. 5.24), because of the fact that on this grid all the triangles are 1-target and in this situation these schemes are all equivalent to the 1-D first order upwind scheme. For this reason there are no differences in the solutions obtained with FCT using either the N scheme as low order or the PSI scheme (fig. 5.25).

The solution obtained by Ferrante using the FCT and the LDA consistent scheme as high order with Crank-Nicolson timestepping is reported in figure 5.26. The results of the

consistent implicit formulation and of the inconsistent explicit method are really close, except for the smearing near the corner present in the latter due to the fact that for this CFL the Lax Wendroff scheme is nearly unstable, and the FCT gives the low order solutions where strong oscillations are present.

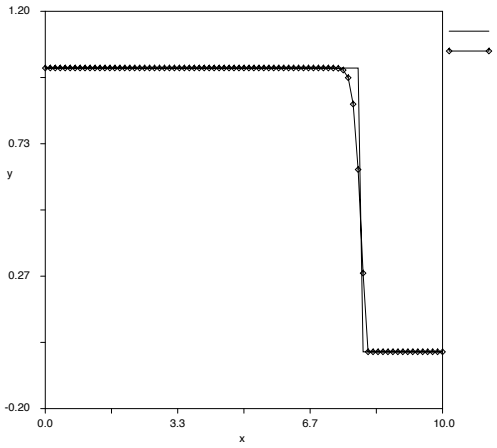

Fig. 5.24 – Low order solution (upwind schemes), $t = 2.95$

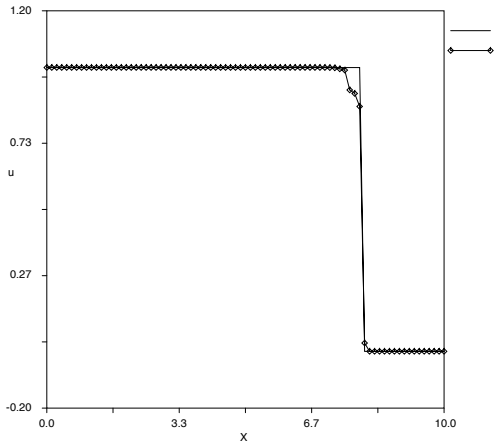

Fig. 5.25 – FCT : L-W inconsistent and N (or PSI) inconsistent, $t = 2.95$

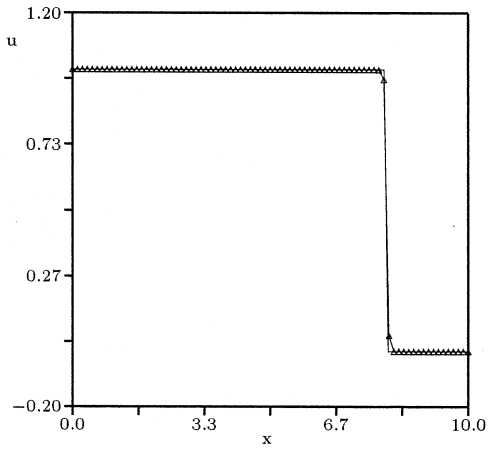

Fig. 5.26 – FCT : LDA consistent and N (or PSI) inconsistent, $t = 2.95$

5.5 1D Burgers' equation

The inviscid Burgers' equation is a non linear scalar advection equation. It is written in the standard form:

$$\frac{\partial u}{\partial t} + \frac{\partial}{\partial x}\left(\frac{u^2}{2}\right) = 0, \tag{5.5}$$

or in quasi linear form:

$$\frac{\partial u}{\partial t} + u\frac{\partial u}{\partial x} = 0, \tag{5.6}$$

The testcase considered here is the same found in [2], i.e. an expansion fan developing from the initial solution:

$$\begin{cases} u_L = -1.5 & x < 5.0, t = 0 \\ u_R = 0.02 & x > 5.0, t = 0 \end{cases} \tag{5.7}$$

This test case has been computed using the 2D code on a 2D regular triangular mesh (fig.5.23) imposing the y component of the velocity vector to be zero and applying the conservative linearization:

$$\vec{\bar{\lambda}} = \frac{1}{S_T}\iint_T \frac{\partial \vec{F}}{\partial u}\, d\Omega = \frac{\partial \vec{F}}{\partial u}(\bar{u}) = \bar{u}\vec{1}_x \tag{5.8}$$

where

$$\vec{F}(u) = \left(\frac{u^2}{2}, 0\right) \tag{5.9}$$

and the average state $\bar{u}$ over a triangular cell is simply given by the arithmetic average:

$$\bar{u} = \frac{u_1 + u_2 + u_3}{3}. \tag{5.10}$$

since $\frac{\partial \vec{F}}{\partial u}$ is linear in u.

The CFL adopted (referred to the maximum absolute value of speed 1.5) is .95, and the time level at which we show the solution is 2.77 after 35 constant time steps.

Like in the 1-D step advection testcase all the lumped upwind schemes gave the same solution (fig. 5.27), while the results with the FCT using the time accurate Lax Wendroff scheme are in figure 5.28. The result obtained in [2] is reported in figure 5.29. For this testcase consistent and inconsistent formulations give nearly the same solution, although the implicit computations give almost the exact solution.

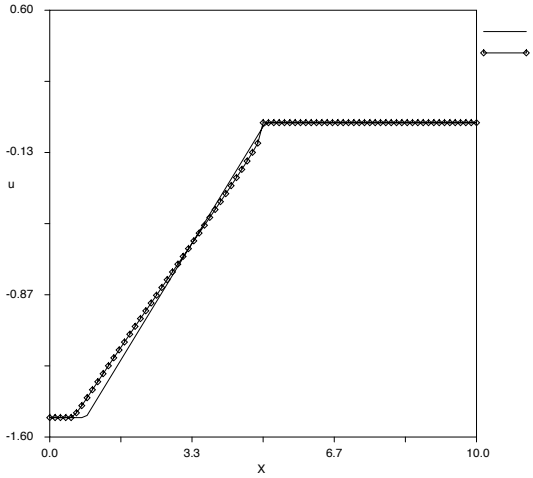

Fig. 5.27 – Low order solution (upwind schemes), $t = 2.77$

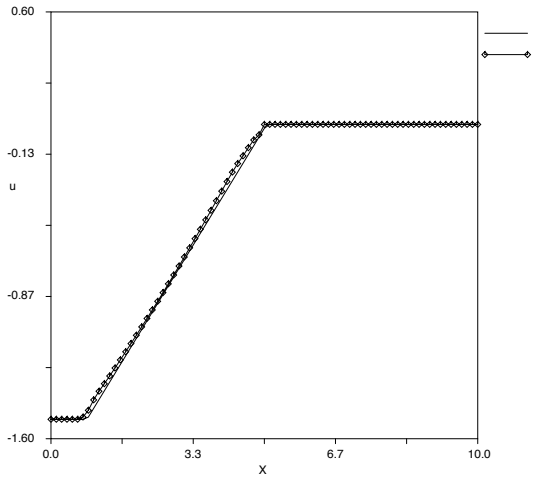

Fig. 5.28 – FCT : L-W inconsistent and N (or PSI) inconsistent, $t = 2.77$

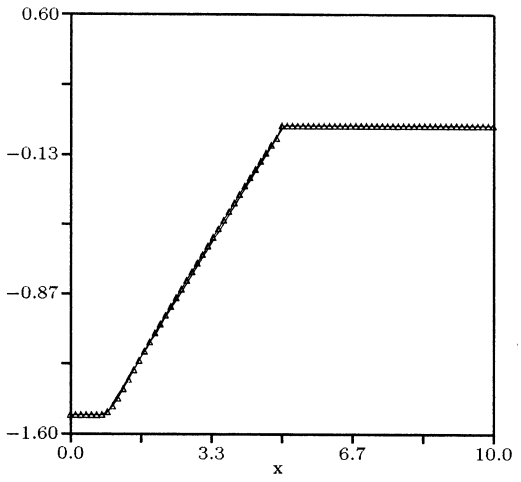

Fig. 5.29 – FCT : LDA consistent and N (or PSI) inconsistent, $t = 2.77$

Part II

2D Euler equations

1. 2D EULER EQUATIONS

The unsteady inviscid compressible flows are governed by the unsteady Euler equations, which in 2D are a hyperbolic non-linear and non-diagonalizable system. This system of equations expresses the conservation of mass, momentum and energy in a compressible, inviscid and non-conducting flow. In conservative form and in two dimensions:

$$\frac{\partial \mathbf{U}}{\partial t} + \frac{\partial \mathbf{F}}{\partial x} + \frac{\partial \mathbf{G}}{\partial y} = 0, \tag{1.1}$$

where $\mathbf{U}$ is the vector of conserved variables, and $\mathbf{F}$ and $\mathbf{G}$ the inviscid fluxes,

$$\mathbf{U} = \begin{pmatrix} \rho \\ \rho u \\ \rho v \\ \rho E \end{pmatrix}, \quad \mathbf{F} = \begin{pmatrix} \rho u \\ \rho u^2 + p \\ \rho uv \\ \rho uH \end{pmatrix}, \quad \mathbf{G} = \begin{pmatrix} \rho v \\ \rho uv \\ \rho v^2 + p \\ \rho vH \end{pmatrix}. \tag{1.2}$$

ρ represents the gas density, u and v are the x- and y-components of the velocity vector $\vec{u}$, p is the static pressure, and E and H are the specific total energy and specific total enthalpy. These flow quantities are related by the following equation,

$$H = E + \frac{p}{\rho}. \tag{1.3}$$

The system is closed by the equation of state for a perfect gas,

$$p = (\gamma - 1)\rho \left[E - \frac{1}{2}(u^2 + v^2) \right], \tag{1.4}$$

where γ is the adiabatic exponent, equal to 1.4 for air at moderate temperatures. The speed of sound c needed to compute the Mach number $M = \|\vec{u}\|/c$, is given by

$$c = \sqrt{\frac{\gamma p}{\rho}}, \tag{1.5}$$

and is related to H by the following identity:

$$c^2 = (\gamma - 1) \left[H - \frac{1}{2}(u^2 + v^2) \right]. \tag{1.6}$$

Quasi-linear forms

In conservative variables

To solve the 2-D Euler equations a matrix approach (see ref. [11]) has been used on a quasi-linear formulation of the system. The quasi-linear form in terms of the conservative variables is given by:

$$\frac{\partial \mathbf{U}}{\partial t} + \mathbf{A}\frac{\partial \mathbf{U}}{\partial x} + \mathbf{B}\frac{\partial \mathbf{U}}{\partial y} = 0 \tag{1.7}$$

where $\mathbf{A} = \partial \mathbf{F}/\partial \mathbf{U}$ and $\mathbf{B} = \partial \mathbf{G}/\partial \mathbf{U}$ are the Jacobian matrices.

In symmetrizing variables

Although the jacobian in equation (1.7) can be computed analytically it is more convenient to solve the system using a different set of variables given by:

$$\partial \mathbf{Q} = \begin{pmatrix} \partial p/\rho a \\ \partial u \\ \partial v \\ \partial p - a^2 \partial \rho \end{pmatrix} = \mathcal{A} \partial \mathbf{U}. \tag{1.8}$$

being

$$\mathcal{A} = \frac{\partial \mathbf{Q}}{\partial \mathbf{U}}. \tag{1.9}$$

$\mathbf{Q}$ is called the vector of symmetrizing variables, since upon this transformation, a symmetric system is obtained:

$$\frac{\partial \mathbf{Q}}{\partial t} + \breve{\mathbf{A}} \frac{\partial \mathbf{Q}}{\partial x} + \breve{\mathbf{B}} \frac{\partial \mathbf{Q}}{\partial y} = 0, \tag{1.10}$$

where $\breve{\mathbf{A}} = \mathcal{A}\mathbf{A}\mathcal{A}^{-1}$ and $\breve{\mathbf{B}} = \mathcal{A}\mathbf{B}\mathcal{A}^{-1}$, and are given by

$$\breve{\mathbf{A}} = \begin{bmatrix} u & a & 0 & 0 \\ a & u & 0 & 0 \\ 0 & 0 & u & 0 \\ 0 & 0 & 0 & u \end{bmatrix} \quad \breve{\mathbf{B}} = \begin{bmatrix} v & 0 & a & 0 \\ 0 & v & 0 & 0 \\ a & 0 & v & 0 \\ 0 & 0 & 0 & v \end{bmatrix}. \tag{1.11}$$

With this choice of variables the last equation decouples from the others (see ref. [13]) giving the following scalar convection equation:

$$\frac{\partial S}{\partial t} + \mathbf{u} \cdot \nabla S = 0, \tag{1.12}$$

where $\mathbf{u} = (u, v)$ is the velocity vector and S is related to the thermodynamic entropy:

$$\partial S = \partial \rho - \frac{1}{a^2} \partial p = -\frac{1}{\gamma} \rho \partial (logs). \tag{1.13}$$

Linearization

The linearization used for the computation of the fluxes is based on the assumption that the parameter vector

$$\mathbf{Z} = \sqrt{\rho}\,(1, u, v, H)^{\mathcal{T}} \tag{1.14}$$

varies linearly over each element. Since $\mathbf{F}$ and $\mathbf{G}$ are quadratic in the components of $\mathbf{Z}$ the following relations hold for the linearized fluxes:

$$\hat{\mathbf{F}}_x = \frac{1}{S_T} \iint_T \mathbf{F}_x d\Omega = \left(\frac{\partial \mathbf{F}}{\partial \mathbf{Z}} \right)_{\hat{\mathbf{Z}}} \mathbf{Z}_x, \tag{1.15}$$

$$\widehat{\mathbf{G}}_y = \frac{1}{S_T}\iint_T \mathbf{G}_y d\Omega = \left(\frac{\partial \mathbf{G}}{\partial \mathbf{Z}}\right)_{\widehat{\mathbf{Z}}} \mathbf{Z}_y, \quad (1.16)$$

where $\mathbf{Z}_x$ and $\mathbf{Z}_y$ are constant over a cell and

$$\widehat{\mathbf{Z}} = \frac{\mathbf{Z}_1 + \mathbf{Z}_2 + \mathbf{Z}_3}{3}. \quad (1.17)$$

For the fluctuation one has

$$\mathbf{\Phi}^T = \iint_T (\mathbf{F}_x + \mathbf{G}_y)\ d\Omega = S_T\ \left[\left(\frac{\partial \mathbf{F}}{\partial \mathbf{Z}}\right)_{\widehat{\mathbf{Z}}} \mathbf{Z}_x + \left(\frac{\partial \mathbf{G}}{\partial \mathbf{Z}}\right)_{\widehat{\mathbf{Z}}} \mathbf{Z}_y\right]. \quad (1.18)$$

Nodal updating

The computation of the nodal residual is made in symmetrizing variables and then it is transformed back in conservative variables, i.e.:

$$\mathbf{\Phi}^T_{i,symm} = |\mathbf{B}^T_{i,symm} \mathbf{\Phi}^T_{symm}, \quad (1.19)$$

with

$$\mathbf{\Phi}^T_{symm} = (\mathcal{A})_{\widehat{\mathbf{Z}}} \mathbf{\Phi}^T; \quad (1.20)$$

finally the nodal residual in conservative variables is computed as:

$$\mathbf{\Phi}^T_i = \left(\frac{\partial \mathbf{U}}{\partial \mathbf{Q}}\right)_{\widehat{\mathbf{Z}}} \mathbf{\Phi}^T_{i,symm}. \quad (1.21)$$

The reasons for this choice are:

1. The distribution matrices $|\mathbf{B}^T_i$ usually depend on the linearized jacobian that are easier to handle in symmetrizing variables.
2. The decoupling of the entropy equation allows the use of a pure scalar distribution scheme for this variable .

The explicit time updating for the node i is:

$$\mathbf{U}^{n+1}_i = \mathbf{U}^n_i - \frac{\Delta t}{S_i} \sum_T \mathbf{\Phi}^T_i, \quad (1.22)$$

The description of the consistent formulation of the space discretization for a system of PDEs can be found in [2] while for the implicit time integration one can refer to [14].

2. SYSTEM LAX WENDROFF SCHEME

To test the Lax Wendroff scheme on time dependent problems involving the Euler equations, the time accurate version of the method has to be extended to matrix schemes .This has been made on IcARus where only the local version (see ref. [11]) was implemented before. On triangles, the distribution matrices that generalize the scalar Lax Wendroff distribution coefficient are (ref. [7]):

$$\mathbb{B}_i^{T,LW} = \frac{1}{3}\mathbf{I}_p + \frac{\Delta t}{4S_T}\left(\mathbf{A}n_{i,x} + \mathbf{B}n_{i,y}\right), \tag{2.1}$$

where $\vec{n}_i = n_{i,x}\vec{1}_x + n_{i,y}\vec{1}_y$ are the inward pointing scaled normals, p is the dimension of the system to be solved (i.e. the number of variables that in our case is 3, since the entropy equation is solved by a scalar scheme). $\mathbf{A}$ and $\mathbf{B}$ are the jacobian matrices computed in the current system of variables, so in our case they are the jacobian present in equation (1.10).

No changes were made to the other schemes for which one can refer to [11].

3. FCT FOR SYSTEMS

The extension of the FCT procedure to non-linear systems is not straightforward. The way it was implemented on IcARus follows the approach found in [12] of computing the limiter as the minimum between a density limiter and an energy limiter. No changes were made to this implementation for the computations carried out here, but the results show that improvement of the limiting must be performed.

A possible method involves the use of the limiting procedure on the decoupled equation 1.12. In fact, since all the results of the first part of this report proved that the FCT guarantees fully monotone results for scalar advection problems. Hence, computing the limiter using the entropy equation (1.12) a monotone solution should be obtained at least for this variable. Because of time restrictions this alternative approach could not be tested in the course of this work.

4. RESULTS

Two testcases have been considered to compare the consistent and inconsistent formulations on the Euler equations.

The first testcase is a 1-D expansion wave. Although this is a 1-D problem the computation was made on a 2-D triangular mesh (fig. 5.23) using periodic boundary conditions to avoid gradients in the y direction. An exact solution of this testcase is known and can be found in [9]. The results will be compared also to this solution.

The second computation made is the Mach 3 wind tunnel with a foreward facing step testcase of reference [10].The initial conditions and the set-up of the computations were the same of the reference, except for the fact that there was no special treatment for the corner here.

Both testcases were chosen to test the accuracy of the scheme as well as its stability in the presence of strong discontinuities in the flow, and in both the more diffusive N scheme is used for the low order computations.

4.1 Rarefraction wave

The flow generated from the motion of a piston receding from an initially resting gas is the test considered here. The piston is instantaneously accelerated from zero to a constant velocity $V = u_R$ causing an expansion wave to occur in the gas. The exact algebraic solution can be found in [9] or in [2], while the initial conditions, the speed of the piston and the CFL number were chosen as in [2].

Results are displayed in figures from 4.1 to 4.4 corresponding to time $t = 1.90$, reached with 35 iterations, with a constant timestep corresponding to a CFL number referred to the speed of the piston ($V = 1$), $CFL \sim 0.4$. It is evident that the two solutions are really close to each other and both are close to the exact solution. The consistent formulation with FCT gives again a better solution, closer to the analytical one, but the time accurate Lax Wendroff scheme with FCT gives comparable results although it is used with the inconsistent mass matrix formulation and explicit time-stepping. The solution in not monotone for both the consistent and inconsistent formulations and this could be due to two factors:

1. Already in [2] it was shown that the low order N system scheme is unexpectedly not completely monotone on this testcase;
2. The FCT procedure is acting on variables figuring in non-linear coupled equations and for strong discontinuities it is not able to ensure the complete monotonicity of the results (see ref. [12]).

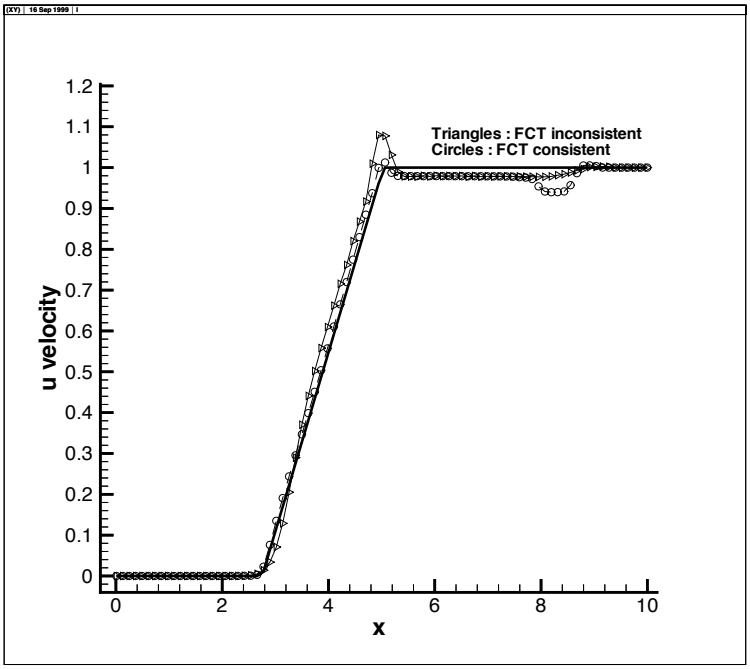

Fig. 4.1 – Velocity u : consistent and inconsistent results at $t = 1.90$ compared with the exact solution

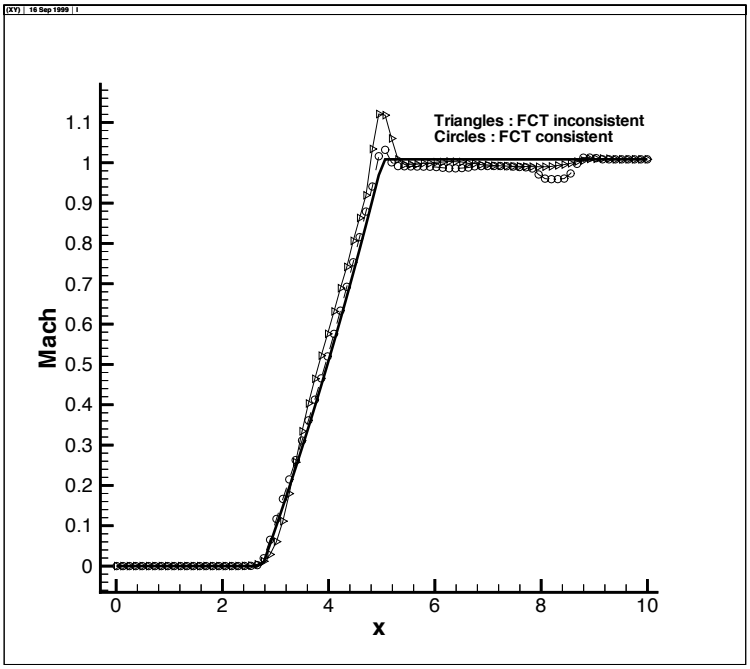

Fig. 4.2 – Mach : consistent and inconsistent results at $t = 1.90$ compared with the exact solution

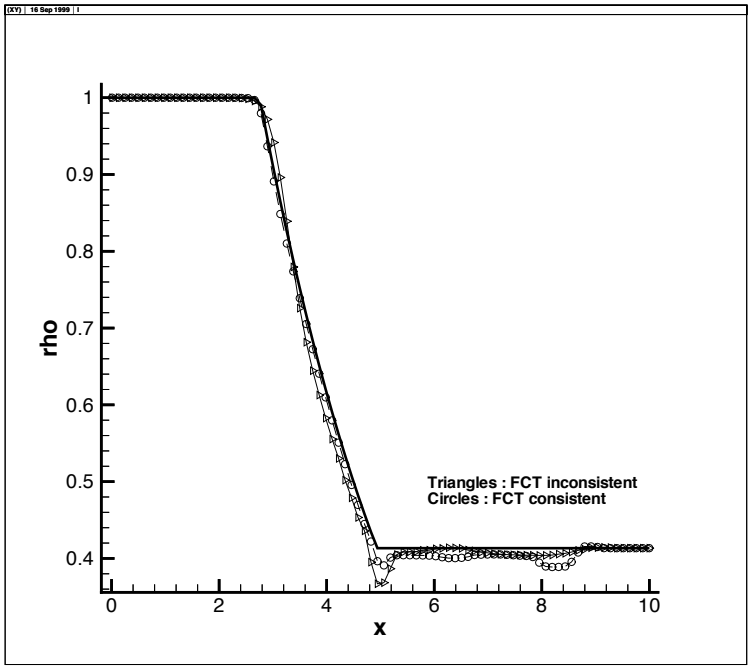

Fig. 4.3 – Density : consistent and inconsistent results at $t = 1.90$ compared with the exact solution

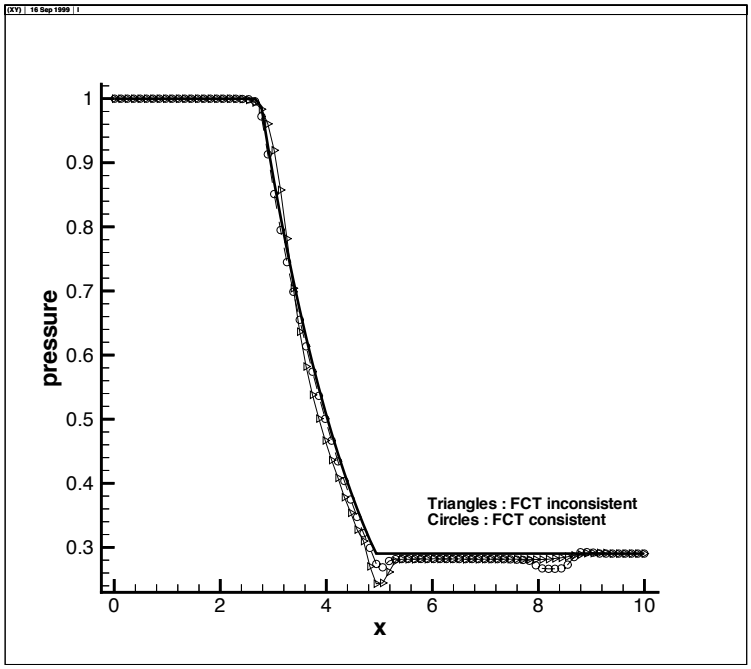

Fig. 4.4 – Pressure : consistent and inconsistent results at $t = 1.90$ compared with the exact solution

4.2 Mach 3 wind tunnel with a foreward facing step

The unsteady shock structures developing from a Mach 3 incoming flow in a wind tunnel with a step is the object of this section. Inviscid wall boundary conditions were imposed all along the step and the upper wall, while supersonic inlet and outlet conditions were given on the inflow and outflow edges. For a more accurate description of the testcase one can refer to [10] or to [2].

The computation was made on the same fine grid used in [2], see (figure 4.5), fixing the same timestep $\Delta t = 1.25 \cdot 10^{-3}$, with a CFL number referred to the incoming uniform flow ($u = 3$), $CFL \sim 0.3$. The results (density contours) obtained with the FCT using inconsistent Lax Wendroff and N scheme with explicit timestepping are displayed in figures from 4.6 on, together with the solution of the reference [10] and with the solution obtained with the FCT using consistent LDA and N scheme with Crank-Nicolson implicit timestepping.

The solution obtained with explicit inconsistent FCT (inconsistent Lax Wendroff and N scheme with explicit timestepping) is not bad also compared to the reference solution.The wiggles in the contour plots could be determined by the weak limiting of the FCT procedure in presence of strong discontinuities and probably by the fact that if a fixed timestep is used, choosing it by a CFL condition based on the incoming flow and not on the actual local value of the velocity, during the computation the CFL condition could be violated locally . To overcome this problem in explicit computations an adaptive timestepping could be implemented, using as a global timestep the minimum between the local timesteps computed imposing locally the CFL condition. The same problem could be at the origin of the instabilities developing in the consistent computation, since in the FCT the low order is computed with explicit timestepping, and if the monotonicity of the low order scheme is lost the monotonicity of the global method is compromised. Pressure and density profiles show that the solution obtained with the inconsistent FCT and the one obtained with the consistent mass matrix formulation are close, although the implicit computations give once more better results, as can be seen from the contour plots. Besides, pressure and density profiles profiles show the really good shock capturing properties of the algorithms used, although is evident that some more work should be done to improve the monotonicity of the schemes, since also for this testcase the FCT works on coupled non-linear equations and, as already said, it is not able to ensure the monotonicity of the solution.

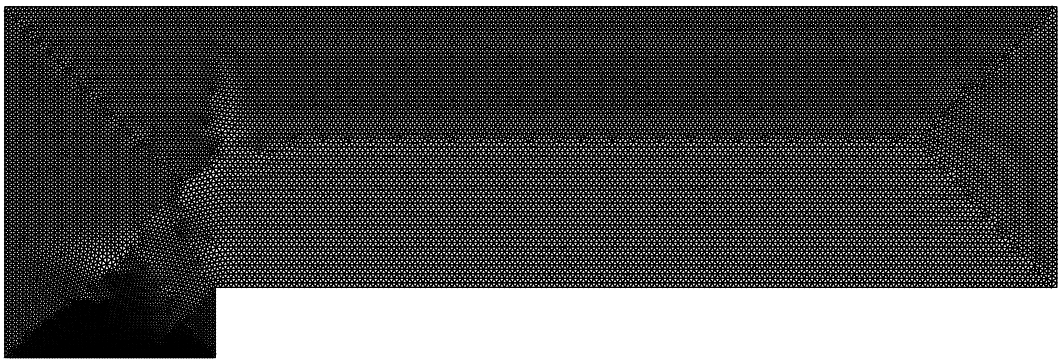

Fig. 4.5 – Grid used for the Mach 3 wind tunnel testcase: 17320 nodes, 33998 cells

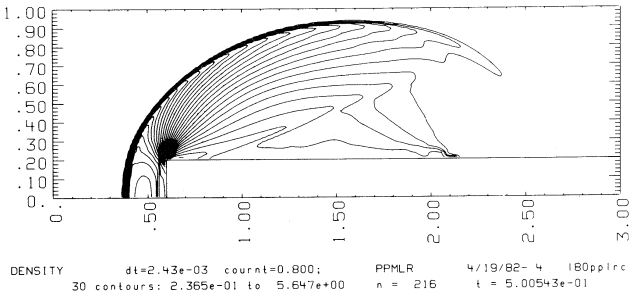

Fig. 4.6 – Reference solution [10], $t = 0.5$

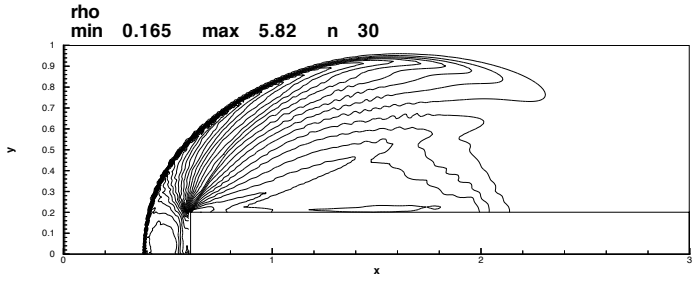

Fig. 4.7 – FCT : L-W inconsistent and N scheme with explicit timestepping, $t = 0.5$

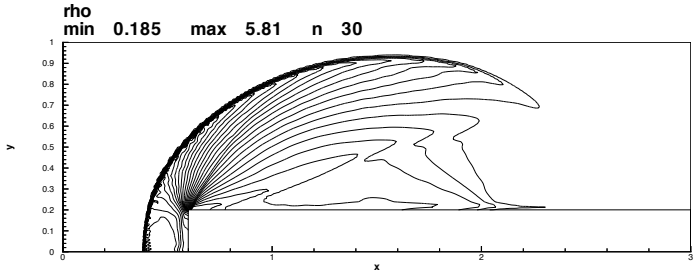

Fig. 4.8 – FCT: consistent LDA with N scheme and Crank-Nicolson timestepping, $t = 0.5$

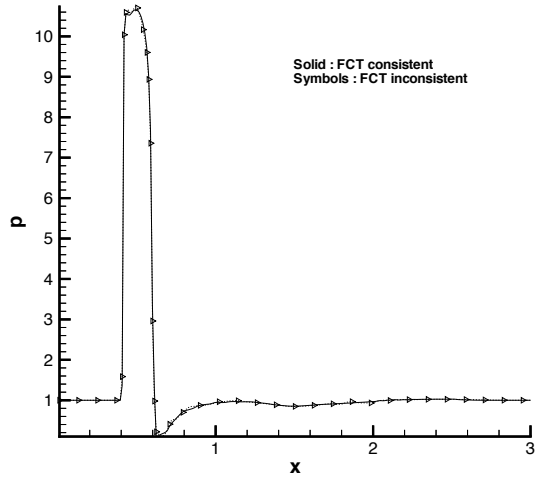

Fig. 4.9 – Pressure profile at $y = 0.2$: comparison between consistent FCT (LDA cons. and N) and inconsistent FCT (L-W incons. and N) at $t = 0.5$

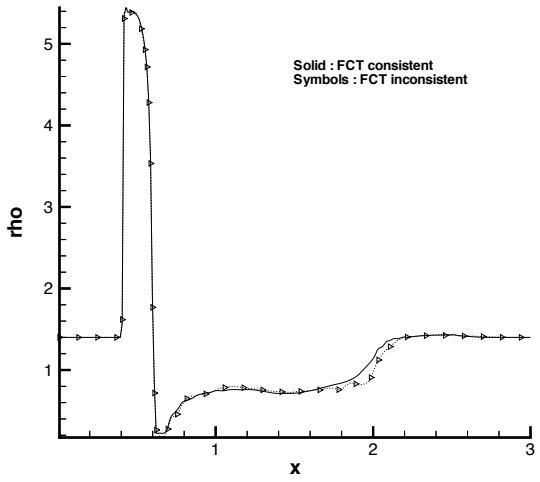

Fig. 4.10 – Density profile at $y = 0.2$: comparison between consistent FCT (LDA cons. and N) and inconsistent FCT (L-W incons. and N) at $t = 0.5$

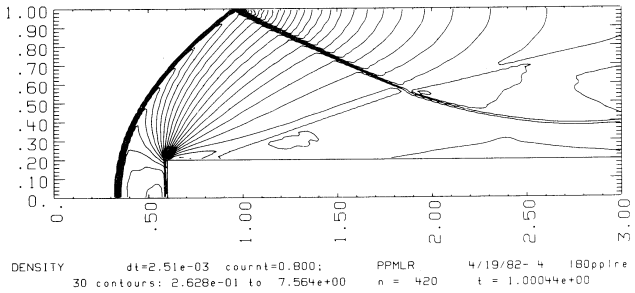

Fig. 4.11 – Reference solution [10], $t = 1.0$

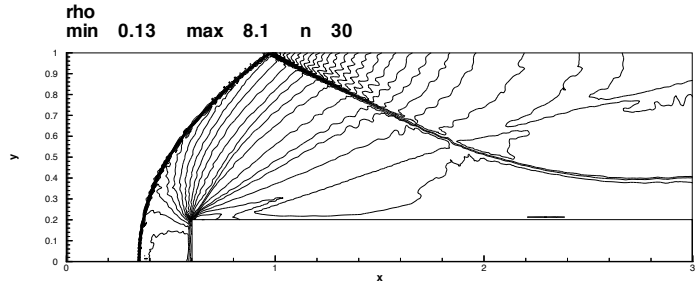

Fig. 4.12 – FCT : L-W inconsistent and N scheme with explicit timestepping, $t = 1.0$

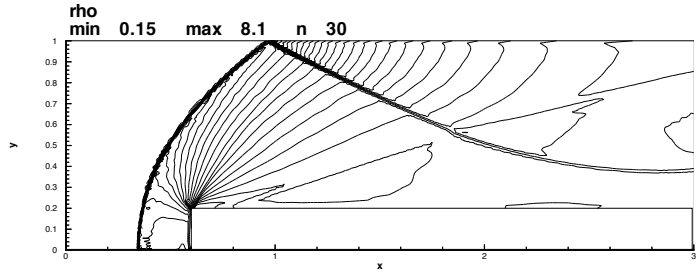

Fig. 4.13 – FCT: consistent LDA with N scheme and Crank-Nicolson timestepping, $t = 1.0$

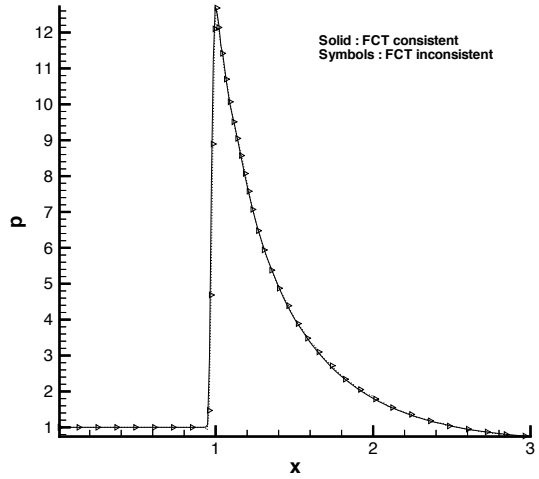

Fig. 4.14 – Pressure profile on the upper wall: comparison between consistent FCT (LDA cons. and N) and inconsistent FCT (L-W incons. and N) at $t = 1.0$

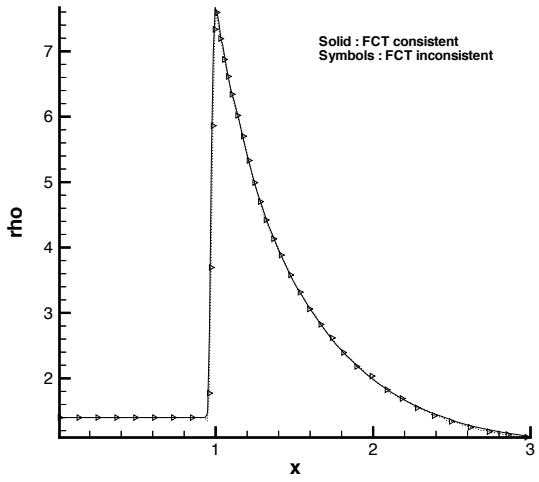

Fig. 4.15 – Density profile on the upper wall: comparison between consistent FCT (LDA cons. and N) and inconsistent FCT (L-W incons. and N) at $t = 1.0$

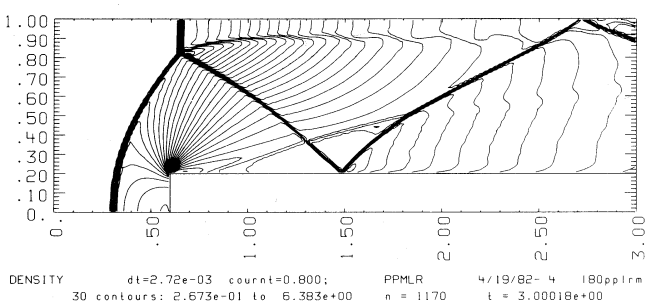

Fig. 4.16 – Reference solution [10], $t = 3.0$

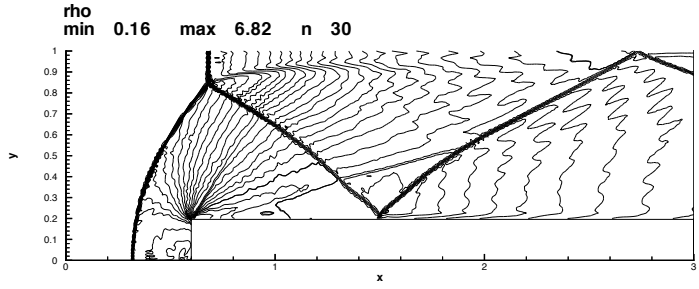

Fig. 4.17 – FCT : L-W inconsistent and N scheme with explicit timestepping, $t = 3.0$

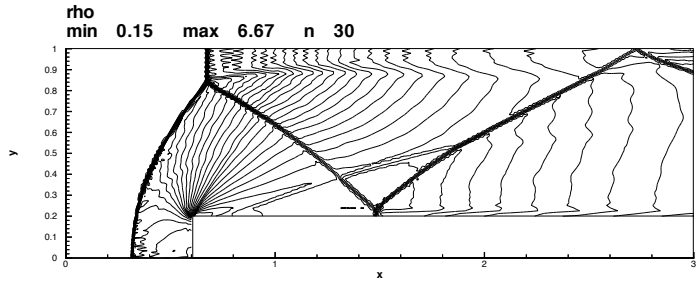

Fig. 4.18 – FCT: consistent LDA with N scheme and Crank-Nicolson timestepping, $t = 3.0$

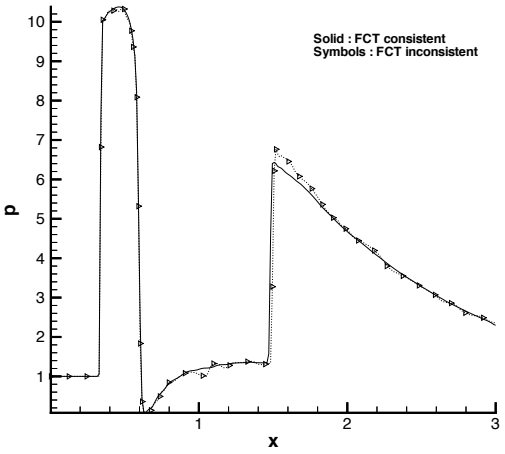

Fig. 4.19 – Pressure profiles at $y = 0.2$, $t = 3.0$

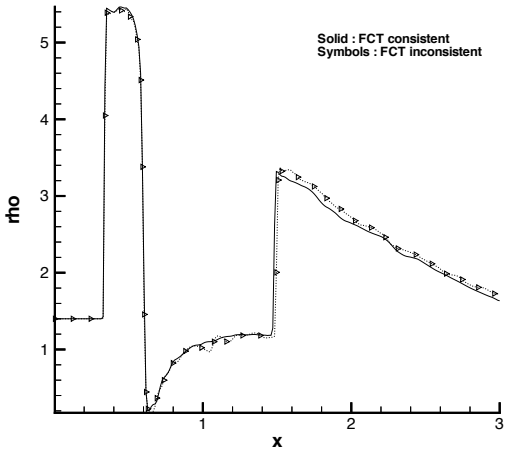

Fig. 4.20 – Density profiles at $y = 0.2$, $t = 3.0$

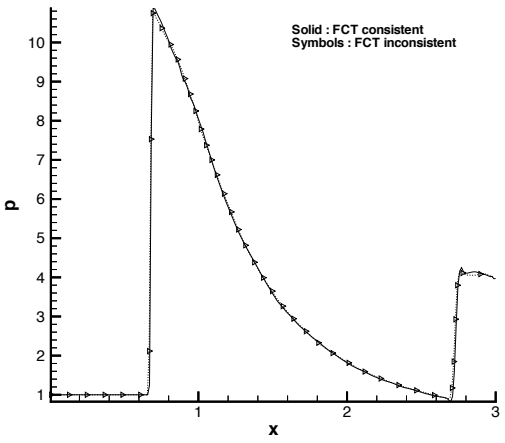

Fig. 4.21 – Pressure profiles on the upper wall, $t = 3.0$

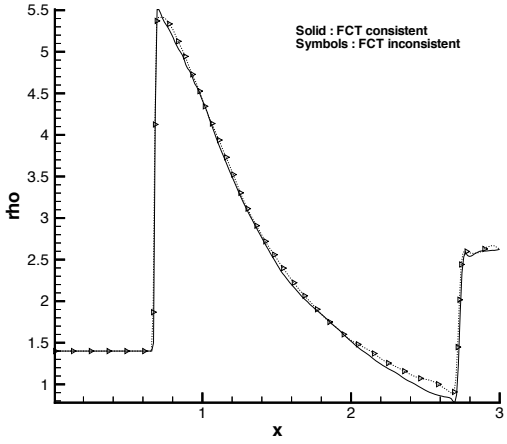

Fig. 4.22 – Density profiles on the upper wall, $t = 3.0$

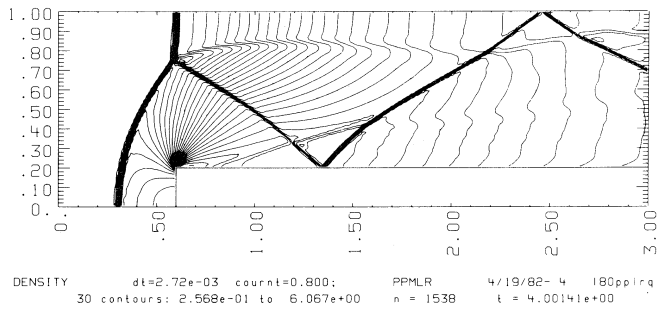

Fig. 4.23 – Reference solution [10], $t = 4.0$

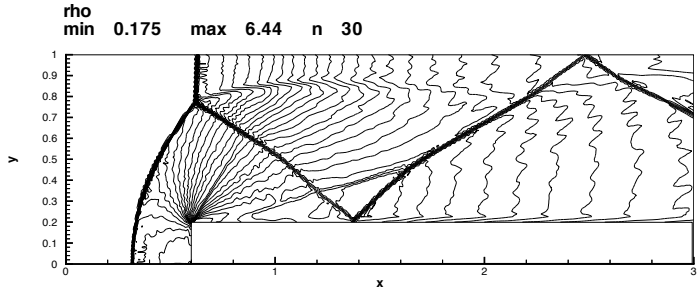

Fig. 4.24 – FCT : L-W inconsistent and N scheme with explicit timestepping, $t = 4.0$

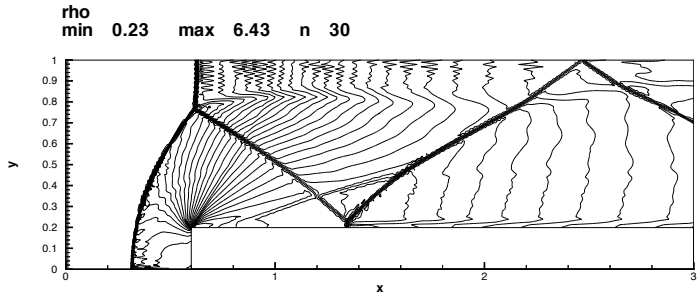

Fig. 4.25 – FCT: consistent LDA with N scheme and Crank-Nicolson timestepping, $t = 4.0$

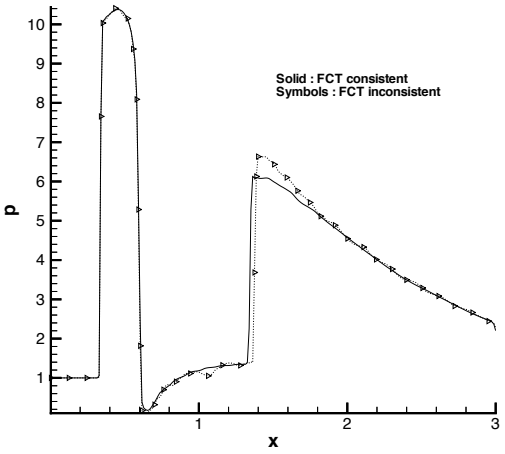

Fig. 4.26 – Pressure profiles at $y = 0.2$, $t = 4.0$

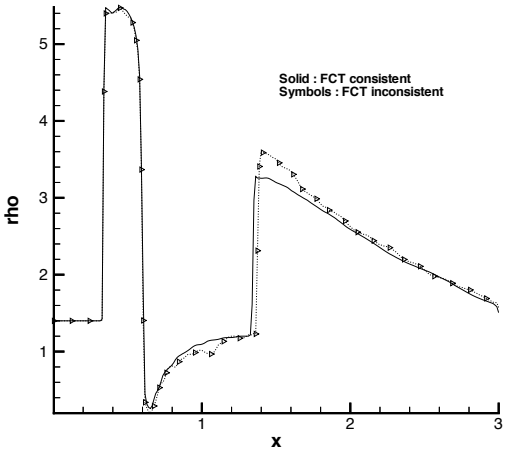

Fig. 4.27 – Density profiles at $y = 0.2$, $t = 4.0$

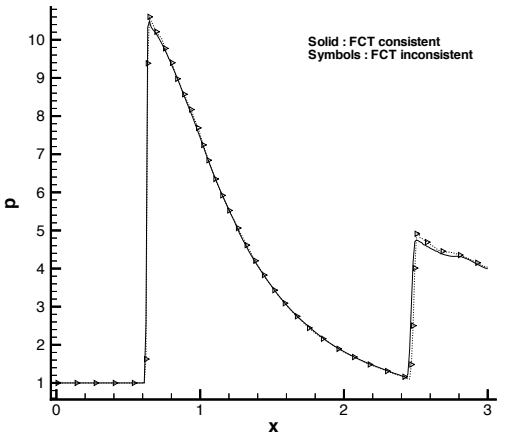

Fig. 4.28 – Pressure profiles on the upper wall, $t = 4.0$

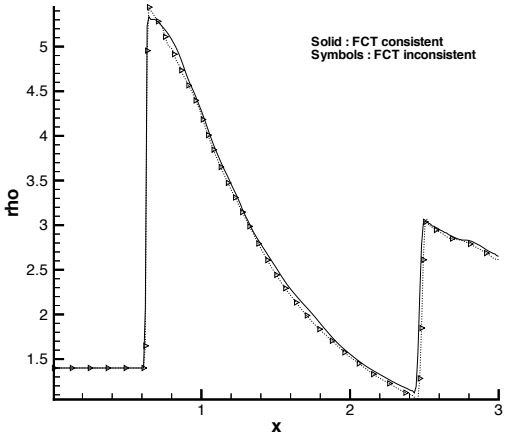

Fig. 4.29 – Density profiles on the upper wall, $t = 4.0$

5. CONCLUSION

An alternative approach for making time accurate computations using fluctuation splitting schemes, based on the use of a Lax Wendroff explicit timestepping, has been tested and compared to the results obtained with an implicit formulation using the consistent mass matrix. The results show that although the explicit formulation gives acceptable results on all the problems computed, the implicit method is always more accurate and often able to give almost the exact solution, at least for scalar computations. Improvements in the solutions obtained with the explicit method could be obtained using finer grids. This however will make the computations more expensive losing the advantage of the explicit timestepping.

On the Euler equations again the implicit method is slightly better than the explicit lumped formulation, but both suffer of a weak limiting of the FCT on coupled non-linear equation, especially in presence of strong discontinuities.

Possible improvements can be made immediately on the code that have not been done here because of the time restrictions:

1. Implementation of an adaptive timestepping based on finding the minimum between the timesteps computed by a locally imposed CFL condition, in order to improve the stability of the explicit low order scheme ;

2. Implementation of the limiting procedure in symmetrizing variables on the decoupled entropy equation (1.12);since on scalar equations the FCT procedure ensures monotonic behavior also in presence of discontinuities, this should improve the monotonicity for Euler equations;

3. Investigation of the possibility of an alternative formulation of the Euler equations in wich more decoupled equations appear (like in the steady preconditioned case) so that the limiting can be done on these equations.

REFERENCES

1. J. Maerz, Improving time accuracy for residual distribution schemes, Project Report 1996-17, June 1996

2. A.Ferrante, Solution of the Unsteady Euler equations using Residual Distribution and flux corrected transport, Project Report 1997 ,June 1997

3. J.P.Boris and D.L.Book, Flux corrected transport. I.SHASTA, atransport algorithm that works, Journal Computational Physics 11 (1973)

4. S.T.Zalesak, Fully multidimensional flux-corrected transport algorithm for fluids, Journal Computational Physics 31 (1979)

5. M.E.Hubbard and P.L.Roe, Compact High-Resolution algorithms for time-dependent advection on unstructured grids, Preprint

6. R.Strujis, A multi-dimensional upwind discretization method for the Euler equations on unstructured grids

7. H. Paillère, Multidimensional Upwind Residual Distribution Schemes for the Euler and Navier-Stokes Equations on Unstructured Grids, PhD thesis, Université Libre de Bruxelles, June 1995

8. Ch. Hirsch, Numerical Computation of Internal and External Flows, Vol. 1 , John Wiley & Sons 1990

9. Courant,Friederchs, Supersonic Flow and Shock Waves, Interscience Publishers Inc., New York 1948

10. P.Colella, P.Woodward, The Numerical Simulation of Two-Dimensional Fluid Flow with Strong Shocks, Journal Computational Physics 54 (1984)

11. E. van der Weide and H. Deconinck, Matrix Distribution Schemes for the System of Euler Equations, Euler and Navier-Stokes Solvers using Multi-dimensional Upwind-Schemes and Multigrid acceleration, Notes on Numerical Fluid Mechanics, Vieweg 1996

12. R. Lohner, K. Morgan, J. Peraire and M.Vahdati, Finite element flux-corrected transport (FEM-FCT) for the Euler and Navier-Stokes equations, International Journal for Numerical Methods in Fluids, vol.7, 1093-1109 (1987)

13. A.Bonfiglioli and H.Deconinck, Multidimensional Upwind Schemes for the 3-D Euler Equations on Unstructured meshes, Euler and Navier-Stokes Solvers using Multi-dimensional Upwind-Schemes and Multigrid acceleration, Notes on Numerical Fluid Mechanics, Vieweg 1996

14. E.Issman, Implicit Solution Strategies for Compressible Flow Equations on Unstructured Meshes, PhD thesis, Université Libre de Bruxelles, October 1997